Identification of client iron-sulfur proteins of the chloroplastic NFU2 transfer protein in Arabidopsis thaliana

Nathalie Berger, Florence Vignols, Jonathan Przybyla-Toscano, Mélanie Roland, Valerie Rofidal, Brigitte Touraine, Krzysztof Zienkiewicz, Jérémy Couturier, Ivo Feussner, Veronique Santoni, et al.

Identification of client iron-sulfur proteins of the chloroplastic NFU2 transfer protein in *Arabidopsis thaliana*

Nathalie Berger[1], Florence Vignols[1], Jonathan Przybyla-Toscano[2], Mélanie Roland[2], Valérie Rofidal[1], Brigitte Touraine[1], Krzysztof Zienkiewicz[3], Jérémy Couturier[2], Ivo Feussner[3,4], Véronique Santoni[1], Nicolas Rouhier[2], Frédéric Gaymard[1], Christian Dubos[1*]

[1] BPMP, Université de Montpellier, CNRS, INRAE, SupAgro, Montpellier, France

[2] Université de Lorraine, INRAE, IAM, F-54000 Nancy, France

[3] Department of Plant Biochemistry, Albrecht-von-Haller-Institute for Plant Sciences and Göttingen Center for Molecular Biosciences (GZMB), University of Göttingen, 37077 Göttingen, Germany

[4] Service unit for Metabolomics and Lipidomics, Göttingen Center for Molecular Biosciences (GZMB), University of Göttingen, 37077 Göttingen, Germany

NB: nathalie.berger@inra.fr; FV: florence.vignols@supagro.fr; JP-T: jonathan.przybyla-toscano@univ-lorraine.fr; MR: Melanie.Roland@univ-lorraine.fr; VR: valerie.rofidal@inra.fr; BT: brigitte.touraine@inra.fr; KZ: krzysztof.zienkiewicz@biologie.uni-goettingen.de; JC: jeremy.couturier@univ-lorraine.fr; IF: ifeussn@uni-goettingen.de; VS: veronique.santoni@inra.fr; NR: Nicolas.Rouhier@univ-lorraine.fr; FG: frederic.gaymard@inra.fr; CD*: corresponding author, christian.dubos@inra.fr, Tel: 0033499612818

Highlights

The present study delineates the interaction network of NFU2, a factor required for the maturation of several chloroplastic Fe-S proteins, extending its previous assigned function in photosystem I assembly.

Abstract

Iron-sulfur (Fe-S) proteins have critical functions in plastids, participating notably in the photosynthetic electron transfer, sulfur and nitrogen assimilation, chlorophyll metabolism and vitamin or amino acid biosynthesis. Their maturation relies on the so-called SUF assembly machinery. The Fe-S clusters are synthesized *de novo* on a scaffold protein complex and then delivered to client proteins *via* several transfer proteins. However, the maturation pathways of most client proteins and their specificities towards transfer proteins are mostly unknown. In order to decipher the proteins interacting with the Fe-S cluster transfer protein NFU2, one of the three plastidial representatives found in *Arabidopsis thaliana*, we have performed a quantitative proteomic analysis of *nfu2* plants (shoots, roots and seedlings). Combined with NFU2 co-immunoprecipitation and binary yeast two-hybrid experiments, we identified 14 new targets, among which nine were validated *in planta* using a binary bimolecular fluorescence complementation (BiFC) assay. These analyses also revealed a possible role for NFU2 in plant response to desiccation. Altogether this study delineates better the maturation pathways of many chloroplastic Fe-S proteins, extending considerably the number of NFU2 clients. It also helps clarifying the respective roles of the three NFU paralogs, NFU1, NFU2 and NFU3.

Key words: NFU2, chloroplast, quantitative proteomic, iron-sulfur cluster, Arabidopsis, protein-protein interactions

INTRODUCTION

Iron is essential for both prokaryotic and eukaryotic organisms as this metal is found in cofactors contributing to the activity and/or stability of metalloproteins involved in key physiological processes (*e.g.* respiration, photosynthesis, DNA repair and replication, sulfur and nitrogen assimilation) (Balk & Pilon, 2011). As a cofactor moiety, iron is mainly found in hemes and in iron-sulfur (Fe-S) clusters, the latter comprising iron atoms and inorganic sulfides (Balk & Schaedler, 2014). In plants, as in other organisms, the most widespread clusters are, in the following order, the [4Fe-4S], [2Fe-2S], Rieske-type [2Fe-2S] and [3Fe-4S] clusters (Pilon *et al.*, 2006; Couturier *et al.*, 2013).

The majority of Fe-S proteins found in plants are encoded by the nuclear genome and organellar proteins are thus imported from the cytosol to dedicated cell compartments as apo-proteins (without of Fe-S cluster). After their targeting, apo-proteins acquire their Fe-S cluster and are converted to mature holo-forms. This maturation step is ensured by the action of complex protein machineries. In *Arabidopsis thaliana*, three machineries for Fe-S cluster assembly have been identified and are distributed in the cytosol (CIA for cytosolic iron-sulfur protein assembly), the mitochondria (ISC for iron sulfur cluster) and the chloroplasts (SUF for sulfur mobilization). The *de novo* building of an Fe-S cluster on so-called scaffold proteins depends on an assembly complex, the composition of which differs as a function of the machinery considered. However, this step requires (i) a cysteine desulfurase that provides sulfur atoms and is associated to other accessory/regulatory proteins, (ii) an electron donor that reduces notably the sulfane sulfur species into sulfide and (iii) an iron donor (still unidentified for the three machineries). After its assembly, the Fe-S cluster is transferred to recipient apo-targets with the help of Fe-S cluster transfer proteins and eventually of chaperones (Balk & Schaedler, 2014).

Within the SUF machinery, 10 proteins in Arabidopsis have been proposed to participate in the transfer of preformed Fe-S clusters: GRXS14, GRXS16, BOLA1, BOLA4, SUFA1, IBA57.2, HCF101, NFU1, NFU2, and NFU3 (Couturier *et al.*, 2013; Przybyla-Toscano *et al.*, 2018). So far, there are no described *bola1*, *bola4* or *iba57.2* mutants, and the Arabidopsis *grxs14*, *grxs16*, *sufa1* and *nfu1* null mutants present no obvious phenotype (Yabe & Nakai, 2006; Rey *et al.*, 2017; Touraine *et al.*, 2019). It is thus difficult to determine the precise functions of these proteins *in planta*. However, both glutaredoxin (GRX) isoforms, GRXS14 and S16, and SUFA1 were characterized *in vitro* as [2Fe-2S] cluster incorporating proteins able to transfer their cluster to an apo-ferredoxin (Bandyopadhyay *et al.*, 2008; Abdel-Ghany

et al., 2005). Moreover, GRXS14 is able to transfer its [2Fe-2S] cluster to SUFA1 *in vitro* suggesting a potential *in vivo* sequential Fe-S cluster shuttling similar to the one described for mitochondrial orthologs (Mapolelo *et al.*, 2013; Banci *et al.*, 2014; Brancaccio *et al.*, 2014). Interestingly, NFU1 also interacts with SUFA1 (Roland *et al*., 2020). As NFU1 is a [4Fe-4S] cluster containing protein, an Fe-S cluster conversion is required if an exchange occurs. For other transfer proteins from the SUF machinery, the corresponding mutants have strong phenotypes. The Arabidopsis *hcf101* mutant is seedling lethal but could be partially rescued when grown with exogenous supply of sucrose. The *nfu2* and *nfu3* single mutants are dwarf and a double mutant is lethal (Lezhneva & Meurer, 2004; Stockel & Oelmuller, 2004; Touraine *et al.*, 2004; Yabe *et al.*, 2004; Nath *et al.*, 2016). These strong phenotypes have been primarily explained by a defect in PSI assembly attributed to defaults in the maturation of the three [4Fe-4S] clusters bound to PsaA, PsaB and PsaC. In the current model, NFU2 and NFU3 act immediately upstream of HCF101 which serves, in this context, as a relay for the final delivery of these [4Fe-4S] clusters (Touraine *et al.*, 2019).

A few studies relying on both *in vitro* and *in vivo* approaches already provided evidence for direct interactions between NFU2 and some partners. Among chloroplastic NFU proteins, NFU2 is to date the sole isoform having the capacity to bind either a [2Fe-2S] cluster or a [4Fe-4S] cluster (Gao *et al.*, 2013). So far, NFU2 was shown to transfer a [2Fe-2S] cluster *in vitro* to GRXS16, to the adenosine 5'-phosphosulfate reductase 1 (APR1) involved in sulfate assimilation and to the dihydroxyacid dehydratase (DHAD) involved in the synthesis of branched chain amino acids (Gao *et al.*, 2013; Gao *et al.*, 2018). Consistent with the latter interaction and the absence of detectable amounts of NFU3 and HCF101 in roots, a short root phenotype is observed in the Arabidopsis *nfu2* mutant that accumulates branched chain amino acid precursors (Stockel & Oelmuller, 2004; Touraine *et al.*, 2019).

There are currently 51 plastidial proteins in Arabidopsis for which there is evidence or prediction that they contain Fe-S clusters and for a large majority, the specificities in the delivery of Fe-S clusters from scaffold proteins is still unknown (Balk & Schaedler, 2014). This was hampered for several reasons, *e.g.* the absence of phenotypes in several mutants for SUF components maybe due to some redundancies, the lack of antibodies for many targets, and the lack of studies addressing direct physical interactions. In the case of *hcf101*, *nfu2* and *nfu3* mutants, we hypothesize that the strong photosynthetic defects mask the existence of other Fe-S protein targets.

Hence, we aimed in the present study at unveiling the set of NFU2 interacting proteins by combining several approaches. A global label free quantitative (LFQ) proteomic strategy was carried out to compare the shoot, root and seedling proteomes of WT and *nfu2* Arabidopsis plants as it is documented that apoforms are often less stable than holoforms and thus subject to degradation. This was completed by the use of untargeted (Co-IP MS/MS, co-immunoprecipitation experiments followed by shotgun mass spectrometry) and targeted approaches (Y2H, binary yeast two-hybrid experiments using candidate Fe-S proteins). These three strategies allowed the identification of 14 new NFU2 targets, nine interactions have been validated using bimolecular fluorescence complementation (BiFC) experiments. We also revealed a possible role for NFU2 in the plant response to desiccation. Finally, this study gives new insights into the partial overlapping functions between the three plastidial NFU paralogs.

MATERIALS AND METHODS

Plant material and growth conditions

For proteomic and metabolomic analyses, *nfu2-1* (SALK_039254C) (Touraine *et al.*, 2004) and Col-8 (wild type, WT) seeds were surface sterilized and sown in 0.2 ml tubes containing 0.8% agar prepared in pH 5.5 Hoagland-based solution (1 mM KH_2PO_4, 1 mM KNO_3, 1 mM $MgSO_4$, 5 mM $CaNO_3$, 50 µM H_3BO_3, 0.05 µM $CoCl_2$, 0.05 µM $CuSO_4$, 15 µM $ZnSO_4$, 2.5 µM KI, 50 µM $MnSO_4$, 3 µM Na_2MoO_4). Iron was added as 50 µM Fe^{3+}-EDTA. After 7 days in growth chamber, the extremities of the tubes were cut off prior transfer in 2.5 l opaque recipient in the same medium. Plants were grown for 8 weeks under short day conditions (8h/16h, day/night; 23°C/20°C, day/night) at a light intensity of 160 µmol.m^{-2}.s^{-1} and 65% humidity (Figure S1A). Leaves and roots were harvested and stored at -80°C until analysis. For abscisic acid (ABA) measurement and rapid dehydration tests, plants were cultivated as described above. Two-week-old seedlings, grown as described in Gao *et al*. (2019), were also included in the proteomic analysis (Figure S1B). For co-immunoprecipitation (Co-IP) experiments, transgenic plants expressing a chloroplastic GFP (*Pro35S:CTP$_{NFU3}$:GFP* in WT) and *nfu2-1* lines complemented by a NFU2:GFP fusion (*Pro35S:NFU2:GFP*) were grown on MS/2 as in Gao *et al*. (2019) (Figure S2).

Constructs

All the PCR products were obtained using high-fidelity DNA polymerase (Phusion) and each construct was sequenced to ensure its integrity. The primers used are described in Table S1.

To generate the *Pro35S:CTP$_{NFU3}$:GFP* construct, the *NFU3* chloroplast targeting sequence, whose length was determined based on public mass spectrometry data (Rowland *et al.*, 2015), was expressed under the control of the cauliflower mosaic virus (CaMV) constitutive 35S promoter (*Pro35S*) and fused with GFP using the pGWB505 vector (Nakagawa *et al.*, 2007).

To generate the *Pro35S:NFU2:GFP*, the *NFU2* cDNA was cloned upstream of the GFP marker and expressed under the control of *Pro35S* in the pGWB505 vector. The coding sequences of *NFU2* and of its target proteins were cloned by PCR, enzymatic restriction, and ligation in pGADT7 and pGBKT7 vectors (Clontech) for Y2H and in pUC-SPYNE and pUC-SPYCE vectors (Walter *et al.*, 2004) for BiFC experiments.

Chlorophyll and carotenoid determination

Two-week-old seedlings (10 per repeat) were sampled and mixed in 100% acetone for pigment extraction in the dark under agitation until the samples get cleared (3 to 4 h). Absorbance of the supernatant was measured at 470, 644.8 and 661.6 nm. The concentrations were determined as follows: Chla (µg/ml)= $11.24*A_{661.6}$ - $2.04*A_{644.8}$; Chlb (µg/ml)= $-4.19*A_{661.6}$ $+20.13*A_{644.8}$; carotenoids (µg/ml)= $(1000*A_{470}$ -1.9*Chla – 63.14 Chlb)/214 (Lichtenthaler, 1987).

Rapid dehydration assay

Three rosettes of 60-day-old plants grown in hydroponic conditions were cut from the root system and water loss was measured as previously described (North et al., 2005).

Phytohormone and metabolite measurements

Extraction of phytohormones was carried out with methyl-*tert*-butyl ether (MTBE) as described by (Herrfurth & Feussner, 2020). Reversed phase separation of constituents was performed as previously described using an ACQUITY UPLC® system (Waters Corp., Milford, MA, USA) equipped with an ACQUITY UPLC® HSS T3 column (100 mm x 1 mm, 1.8 µm; Waters Corp., Milford, MA, USA). Nanoelectrospray (nanoESI) analysis was carried out as described earlier (Herrfurth & Feussner, 2020) and phytohormones were ionized in a negative mode and determined in a scheduled multiple reaction monitoring mode

with an AB Sciex 4000 QTRAP® tandem mass spectrometer (AB Sciex, Framingham, MA, USA). Mass transitions not listed in Herrfurth & Feussner (2020) are given below:

NRM transitions		***Analyte***	***DP (declustering potential)***	***EP (entrance potential)***	***CE (collision energy)***
Q1	***Q3***				
137	93	SA	-25	-6	-20
141	97	D4-SA	-25	-6	-22
174	130	IAA	-55	-4	-16
179	135	D5-IAA	-35	-9	-14
263	153	ABA	-35	-4	-14
293	179	D6-ABA	-80	-10	-42

Protein extraction and trypsin digestion for label free experiments

Proteins were extracted from 50 mg of leaves or roots from eight weeks old plants and of seedlings from two weeks old plants in 250 µl of 1X Laemmli (65 mM Tris-HCl pH 7.5; 5% glycerol; 2% SDS) (Laemmli, 1970). After vortexing, samples were centrifuged at 20°C for 10 min at 14,000 g. The supernatant was withdrawn and protein content was measured using the Pierce™ Detergent Compatible Bradford Assay Kit (ThermoScientific) (Bradford, 1976). 35 µg of extracted proteins for each sample were loaded on a 12% pre-casted gel (Bio-Rad) and were subject to a 20 min migration at 100 V. Each lane of the gel was cut in 4 parts and in small pieces (2 mm^2), washed two times with carbonate buffer (**25 mM NH_4HCO_3) and two other times with 50% acetonitrile in 25 mM NH_4HCO_3. Bands were dehydrated in 100% acetonitrile and after drying, treated during 45 min at 56°C with 10 mM DTT, and alkylated with 55 mM iodoacetamide during 30 min at room temperature in the dark. Treated bands were washed two times with 50% acetonitrile in 25 mM NH_4HCO_3 and were dehydrated in 100% acetonitrile. After drying, samples were digested with a trypsin solution (Sequencing Grade Modified Trypsin, Promega, Madison, USA), in a 1:50 (trypsin:protein) ratio overnight at 37°C. Peptides were extracted from the gel with 200 µl of 2% formic acid (FA) under shaking during 30 min. The supernatant was collected and two more extractions were done with 80% acetonitrile / 2% FA under shaking, during 30 min each. The three supernatants were pooled and vacuum dried.**

Each sample was solubilized in 10 µl of 2% FA and 1 µl were injected for mass spectrometry (MS/MS) analysis (Qexactive Plus, ThermoFisher Scientific, Waltham, MA, USA).

Data processing for protein identification and label free quantification (LFQ)

Raw mass spectrometric data were analyzed in the Maxquant environment (Cox & Mann, 2008) v.1.5.0.0 and Andromeda was employed for database search (Cox et al., 2011). The MS/MS data were matched against the TAIR10 + GFP database. For protein identification and quantification, cysteine carbamidomethylation was set up as fixed modification and oxidation of methionine as a variable modification. At least two peptides are necessary for protein identification and quantification. Up to two missed cleavage was allowed for protease digestion. For other characteristics, Maxquant default parameters were used. Following the quantification step and the LFQ normalization, proteins were considered as quantifiable only if they are present in all samples. Data were log2 transformed prior analysis. For statistics, pairwise t-tests P<0.05 were carried out. Before statistical treatment, the normal distribution of the logarithmic transformed data was assessed.

For present/absent analysis, a protein was considered as absent in nfu2-1 if it was identified with 2 peptides in at least 3 WT replicates and not in the 4 nfu2-1 replicates.

All raw MS data and Maxquant files generated have been deposited to the ProteomeXchange Consortium via the PRIDE partner repository with the dataset identifier PXD015624.

Co-IP MS/MS experiments

One g of aerial tissues from 2-week-old seedlings was crosslinked in 1% formaldehyde in phosphate buffered saline solution (137 mM NaCl, 10 mM Phosphate, 2.7 mM KCl, and a pH of 7.4) two times (7 min under vacuum). The reaction was blocked by adding 300 mM glycine (30 min under vacuum). Fixed tissues were rinsed three times with water, dried and frozen in liquid nitrogen prior grinding. Powder was diluted in 2 ml of RIPA buffer (50 mM Tris-HCl, pH 7.5, 1 mM EDTA, 1% Nonidet P-40, 1% sodium-deoxycholate) and centrifuged two times for 10 min at 14,000g to remove cell debris. 50 µl of antibodies directed against GFP and coupled to magnetic beads (Miltenyi Biotec®) were added to the supernatant and mixed (wheel rotation) for 30 min at 4°C. Tubes were then placed on magnetic rack and after 4 washes with RIPA buffer, proteins were

eluted with 100 µl of 1X Laemmli solution. Samples were then treated and analyzed like for the LFQ with the following parameters: a protein was considered as interacting with NFU2 if it was identified with 2 peptides in at least 2 Pro35S:NFU2:GFP replicates and not in the 3 Pro35S:CTP$_{NFU3}$:GFP replicates. All raw MS data and Maxquant files generated have been deposited to the ProteomeXchange Consortium via the PRIDE partner repository with the dataset identifier PXD015624.

Y2H experiments

All constructs for Y2H assays were prepared in pGADT7 (fusions with Gal4 activation domain AD) and pGBKT7 (fusions with Gal4 DNA binding domain (BD) vectors (Clontech). Primers used for cloning the sequence encoding the mature form of selected proteins are described in Table S1. Yeast CY306 cells (Vignols et al., 2005) were prepared and co-transfected with AD- and BD-based construct pairs as described earlier (Vignols et al., 2005; Couturier et al., 2014; Touraine et al., 2019).

BiFC experiments

All constructs for BiFC assays were prepared in pUC-SPYNE and pUC-SPYCE vectors (proteins with their transit peptide fused upstream of the N-terminal and the C-terminal part of the YFP fluorescent protein, respectively) (Walter et al., 2004). Arabidopsis protoplasts were prepared and co-transfected with pUC-SPYNE and pUC-SPYCE construct pairs for 5 min in a PEG-based medium as described earlier (Yoo et al., 2007) without vacuum infiltration. Pairs of constructs involving one empty vector were also transfected as a control to ensure that none of the proteins assayed could restore YFP fluorescence in the absence of interacting partners. The YFP fluorescence in Arabidopsis protoplasts was recorded between 520 and 550 nm with a SP8 laser-scanning confocal microscope (Leica Microsystems) after excitation with an argon laser at 514 nm. The fluorescence of chlorophyll was recorded between 680 and 720 nm after excitation at 561 nm. Confocal images were obtained at high resolution using the Leica LAS X software and subsequently treated with the Adobe Photoshop CS3 software. Maximum Z-stack intensity projection was used only to image punctuate or low intensity BiFC results. Three independent transfection assays were performed for each protein pairwise, of which effective BiFCs were considered as positive results only when reproduced in all assays (10 to 20 cells routinely analyzed).

RESULTS

Global analysis of the biological function of proteins whose abundance is affected in an nfu2 mutant

To uncover the pathways affected in *nfu2* loss-of-function mutants and to identify new NFU2 targets, label free quantitative (LFQ) proteomic analyses were performed using total protein extracts from two-week-old seedlings as well as from roots and shoots/leaves of eight-week-old Arabidopsis *nfu2-1* mutant and wild type (WT) plants (Figure S1A and S1B). In total, 4616, 3824 and 2393 proteins were identified in roots, leaves and seedlings, respectively from the four replicates using both genotypes. The abundance of 321, 820 and 502 proteins present in roots, leaves and seedlings, respectively varied significantly, displaying a logarithmic fold change (log2(FC)) lower than -0.2 or higher than +0.2 between *nfu2-1* and WT samples (Tables S2 to S4). Among them, 167, 339 and 174 are less accumulated whereas 154, 481 and 328 are more accumulated in *nfu2-1* roots, shoots and seedlings respectively, when compared to the WT. The subcellular localization of these proteins was analyzed using the multiple marker abundance profiling method of the SUBA4 bioinformatic platform (http://suba.live/; Hooper *et al*., 2017) (Figure 1). In eight-week-old *nfu2*-1 roots and leaves, the proteins less accumulated are mainly cytosolic and nuclear (Figures 1A and 1B). This is different from two-week-old seedlings, in which 75% of the proteins are localized in plastids (Figure 1C). Concerning proteins that are more accumulated, about 90% reside in plastids in leaves and seedlings, (Figures 1B and 1C) whereas 30% are predicted as extracellular and 50% have an unassigned localization n *nfu2-1* roots (Figure 1A). Taken together this first analysis suggests that *nfu2-1* mutation, by affecting the amount of several proteins present in chloroplasts, impacts the entire cell organization, strongly modulating the accumulation of cytosolic, nuclear and extracellular proteins, notably in roots.

Gene ontology (GO) term enrichment analysis of the proteins whose abundance varied in *nfu2-1* was conducted using the PANTHER gene ontology platform (http://go.pantherdb.org) (Figure 2, Tables S5 and S6). In root samples, proteins of the oxidative pentose phosphate pathway (OPPP) (GO:0009051), notably glucose-6-phosphate dehydrogenase (G6PDH) and 6-phosphogluconate dehydrogenase (PGD), were over-represented (Figure 2A). For instance, PGD1 and PGD3, both targeted to the cytosol and the plastids, were over-accumulated in *nfu2-1* when compared to the WT (Holscher *et al.*, 2016). The amount of the third isoform, the peroxisomal PGD2, was not affected. These changes suggest that compensatory mechanisms for maintaining the formation of NADPH have been established. The need of

reducing equivalents is notably important for the functioning of antioxidant systems. Hence, the induction of OPPP may correlate with an oxidative stress occurring in *nfu2-1* roots (Juhnke *et al.*, 1996; Stincone *et al.*, 2015). However, this GO term analysis also indicated that the abundance of proteins involved in the response to several other stresses was decreased in *nfu2-1* roots (cadmium ion, GO:0046686; osmotic stress, GO:0006970; abiotic stress, GO:0009628; biotic stress, GO:0009607 and GO:0043207; decreased oxygen levels, GO:0036293, GO:0070482 and GO:0001666). Other GO term enrichments likely recapitulate Fe-S protein maturation defects. The carbohydrate derivative biosynthetic process GO term (GO:1901137) reflects in large part the decrease of isopropyl-malate isomerase complex proteins, the large subunit of the heterodimer (IPMI LSU1) being a known Fe-S protein associated to a small subunit represented by three isoforms. Similarly, the oxidation-reduction process GO term (GO:0055114) gathers cytosolic and chloroplastic Fe-S enzymes implicated in diverse biochemical processes, including aconitase (ACO1), glutamate synthase (GLU2), nitrite reductase (NIR) and sulfite reductase (SIR).

On the other hand, this GO term analysis indicated that the metabolic adjustments/perturbations occurring in *nfu2-1* leaves and seedlings are globally similar (Figure 2B and C). Indeed, these proteome analyses pointed to the establishment of a response to photosynthesis deficiency with over-represented GO terms in the mutant such as rubisco complex assembly (GO:0110102), carbon fixation (GO:0015977), reductive PPP pathway (GO:0019253), but also to a negative regulation of photosynthesis (GO:0043155), which corresponds mainly to the photorespiration process. Accordingly, the photosynthesis (GO:0015979) and the electron transport chain (GO:0022900) GO terms, corresponding in part to photosystem subunits, are enriched among proteins whose abundance is decreased in *nfu2-1* seedlings. Surprisingly, nine enzymes of the tricarboxylic acid (TCA) cycle (GO:0006099 and GO:0072350) had their abundance diminished in *nfu2-1* leaves. This is in contrast to what is usually observed in mutants affected in photosynthesis that display an increase of the TCA cycle protein/activity (Motohashi *et al.*, 2012). Even though the chloroplast ultrastructure is not visibly altered in the *nfu2* mutant (Touraine *et al.*, 2019), another major conclusion arising from this GO term analysis is that there are major perturbations of the chloroplastic functions, which are likely a consequence of the reported photosynthesis failure (Touraine *et al.*, 2019). Indeed, in *nfu2-1* leaves and seedlings, plastid translation (GO:0032544), plastid organization (GO:0009657), and *de novo* protein folding (GO: 0006458) as well as thylakoid membrane organization (GO:0010027) GO terms are enriched in proteins whose abundance was increased.

As observed for roots, the GO terms over-represented in proteins with decreased abundance in *nfu2-1* leaves or seedlings relate globally to the response to stresses with enriched GO terms in leaves such as response to oxidative, abiotic and biotic stresses (Figures 2B and C). Interestingly, in both leaves and seedlings, the most enriched biological functions in this GO term analysis were reminiscent of the response to a water deficit *i.e.*, response to abscisic acid (ABA) and osmotic stress in seedlings and response to desiccation in leaves. All of this suggested that the general stress response mechanisms of the *nfu2-1* mutant are altered but in particular that the ABA signaling and/or metabolism is affected. Carefully looking at the abundance of proteins known to participate to the water deficit response, we observed that the levels of RD2 and RD29A (response to desiccation 2 and 29A), of the dehydrin ERD14 (early response to dehydration 14) and of different LEAs (late embryogenesis abundant) were decreased in *nfu2-1* leaves (Figure 3A). We therefore measured phytohormones as a second proxy to determine whether this may originate from variations in the ABA content. These analyses revealed that among the hormones measured, ABA was the sole for which abundance was decreased in the *nfu2-1* mutant leaves when compared to the WT (Figure 3B and Figure S1C). Rapid dehydration assays showed that water loss was faster for the *nfu2-1* mutant than for the WT (Figure 3C).

Impact of nfu2-1 mutation on photosystem I (PSI) protein components

NFU2 is required for the biogenesis of a functional PSI. Accordingly, a decreased accumulation of proteins constituting the core complex of PSI (PsaA and B), and the peripheral subunits (PsaC, D-1 and D-2) as well as proteins from the peripheral antenna (Lhca-1 to Lhca-4, PSI light harvesting complex protein a 1 to 4) was reported in Arabidopsis *nfu2* mutants using western blot (WB) analyses (Touraine *et al.*, 2004; Yabe *et al.*, 2004; Gao *et al.*, 2013; Hu *et al.*, 2017).

In order to get more insights into the importance of NFU2 in this process, the accumulation of the 31 proteins involved in PSI biogenesis (PSI subunits and maturation factors) was specifically assessed (Table 1). The previous observations made for PsaA, B, C and D-2 as well as for Lhca-1 to Lhca-3 were confirmed in both *nfu2-1* leaves and seedlings. A decrease of PsaD-1 protein accumulation was observed only in *nfu2-1* leaves whereas a decrease Lhca-4 accumulation was solely observed in *nfu2-1* seedlings. Additionally, this approach revealed that PsaF, G, H-2, K, E-1 and N accumulation was decreased in *nfu2-1* leaves and seedlings. PsaL, O, E-2, Lhca-5 protein accumulation was also decreased in the *nfu2-1* mutant, but only in seedlings. In contrast, the levels of a few proteins increased *i.e.*, Lhca-6 and PPD1 (PsbP

domain protein 1) in *nfu2-1* leaves, Ycf3 (hypothetical chloroplast open reading frame 3) in *nfu2-1* seedlings and Ycf4 in both *nfu2-1* leaves and seedlings.

Altogether, 12 proteins from the PSI (≈38%) displayed altered accumulation in the *nfu2-1* mutant, including the three Fe-S proteins (*i.e.* PsaA, B and C). These data confirm that NFU2 activity defect has profound effects on the accumulation of proteins that are involved in PSI biogenesis and architecture.

Quantification of Fe-S proteins in nfu2-1

The major goal of this study was to identify new NFU2 targets among plastidial Fe-S proteins. Among the 51 predicted chloroplastic Fe-S proteins (Przybyla-Toscano et al., 2018), 37 (≈70%) were quantifiable in both WT and one of the *nfu2-1* mutant samples (Table 2).

The abundance of several Fe-S proteins was significantly decreased in the *nfu2-1* mutant, nine in roots (*i.e.* APR2, adenosine 5'-phosphosulfate reductase 2; ASE1 and 2, glutamine phosphoribosyl pyrophosphate amidotransferase 1 and 2; DHAD, dihydroxyacid dehydratase; FTR, ferredoxin:thioredoxin reductase; GLU2; IPMI LSU1; NIR; SIR), eight in leaves (*i.e.* DWARF27.2, beta-carotene isomerase D27; HCF101, high chlorophyll fluorescence 101; GLU2; NDHK, NADH dehydrogenase subunit K; NDHI, NADPH dehydrogenase subunit I; PsaA, B and C) and five in seedlings (*i.e.* GLT1, NADH-dependent glutamate synthase 1; PAO, pheophorbide a oxygenase; PsaA, B and C).

In contrast, three proteins displayed an increased accumulation in *nfu2-1* mutant, NEET in leaves and GLU1 (glutamate synthase 1) and PSB33 (photosystem B protein 33) in both leaves and seedlings. The FTR displayed a contrasted pattern of accumulation as it was decreased in roots and increased in leaves and seedlings. Similarly, the accumulation of SIR in the *nfu2-1* mutant was decreased in roots and increased in leaves.

Altogether, the abundance of 21 different chloroplastic Fe-S proteins was significantly affected in the *nfu2-1* mutant. Importantly, the accumulation pattern of seven of these proteins (*i.e.* HCF101, GLU1, NIR, PsaA, PsaB, PsaC and SIR) was similar to what was described in previous studies (Touraine *et al.*, 2004; Yabe *et al.*, 2004; Gao *et al.*, 2013). Hence, it is likely that the 11 other proteins whose abundance is decreased in *nfu2-1* (*i.e.* APR2, ASE1, ASE2, DWARF27.2, FTR, GLU2, GLT1, IPMI LSU1, NDHK, NDHI and PAO) are novel targets of NFU2.

Co-immunoprecipitation (Co-IP MS/MS) experiments identified new potential NFU2 interacting proteins

With the aim to identify additional NFU2 targets, Co-IP MS/MS experiments were performed using three independent *nfu2-1* transgenic lines overexpressing *NFU2* (*Pro35S:NFU2:GFP*). Noteworthy, the construct is functional as it rescues the *nfu2-1* growth and root length defects (Figure S2). Three independent lines expressing GFP targeted to the chloroplast (*Pro35S:CTP$_{NFU3}$:GFP*) were used as a control (Figure S3).

Following Co-IP MS/MS analysis, a protein was considered as a putative NFU2 interacting protein when (i) it was not detected in the three *Pro35S:CTP$_{NFU3}$:GFP* replicates but present at least in two *Pro35S:NFU2:GFP* replicates, or (ii) when it was present in all the samples but significantly over-represented in the *Pro35S:NFU2:GFP* lines (*t*-test: $P<0.05$). Based on these criteria, 26 proteins were retrieved, among which 25 are predicted as chloroplastic proteins (Table 3). This included six proteins not detected in the three *Pro35S:CTP$_{NFU3}$:GFP* replicates and 20 proteins significantly over-represented in the *Pro35S:NFU2:GFP* lines. Importantly, the GFP was not found as differentially expressed between the lines, confirming the suitability of the used control.

Among these 26 proteins, four known Fe-S proteins GLT1, GLU1, ISPG (4-hydroxy-3-methylbut-2-enyl diphosphate synthase) and ISPH (4-hydroxy-3-methylbut-2-enyl diphosphate reductase) were present. ISPG and ISPH are two enzymes from the non-mevalonate or methyl-erythritol 4-phosphate pathway required for the synthesis of IPP (isopentenyl diphosphate) and DMAPP (dimethylallyl diphosphate), the precursors for several isoprenoid-derived molecules (*e.g.* chlorophylls, carotenoid, ABA). In fact, no variation in GLT1, ISPG and ISPH abundance between *nfu2-1* and WT plants was observed in the LFQ proteomic analyses whereas GLU1 was over-accumulated in *nfu2-1* leaves and seedlings (Table 2). Interestingly, the proteomic analysis revealed that the abundance of three enzymes (*i.e.* DXR, 1-deoxy-d-xylulose 5-phosphate reductoisomerase; ISPD, 4-diphosphocytidyl-2C-methyl-D-erythritol synthase; ISPE, 4-(cytidine 5'-phospho)-2-C-methyl-D-erithritol kinase) acting upstream of ISPG and ISPH was increased in *nfu2-1* leaves. This observation suggests the establishment of compensatory mechanisms to sustain the biosynthesis of these essential compounds and thus to maintain *nfu2-1* growth. To investigate further this hypothesis, two-week-old *nfu2-1* and WT seedlings were treated with fosmidomycin, an inhibitor of DXR activity (Mueller *et al.*, 2000). As expected, a decrease in the chlorophyll and carotenoid contents, fresh weight and primary root growth was observed for the WT (Figure 4). For the *nfu2-1* mutant, the decrease in the chlorophyll and carotenoid

contents followed a similar trend as the WT (Figures 4A and 4B). However, the difference in the fresh weights between the WT and *nfu2-1*, synonymous of its reduced growth, disappears for the highest fosmidomycin concentrations tested (Figure 4C). These data suggest that additional proteins should act redundantly with NFU2 in shoots to sustain Fe-S cluster assembly in ISPG and ISPH. It is also noticeable that unlike WT plants, *nfu2-1* primary root growth was not affected by the fosmidomycin treatment (Figure 4D). These latter observations suggest that the *nfu2-1* mutant has already minimal levels of isoprenoid precursors and that NFU2 function in sustaining primary root growth occurs *via* its involvement in the biosynthesis of isoprenoid precursors.

Targeted binary yeast two-hybrid (Y2H) screen

Although powerful, the LFQ proteomic approach did not allow detecting all proteins and the Co-IP MS/MS experiments do not necessarily provide information about direct physical interactions. Moreover, despite the use of a cross-linker before protein immunoprecipitation, it can be challenging to detect weak or transient interactions with the latter approach. Thus, complementary Y2H experiments were carried out in parallel to test the interactions between NFU2 and selected [4Fe-4S] chloroplastic proteins, most of them already tested with NFU1 (Roland *et al.*, 2020). It included ASE2, the three DWARF27 paralogs, IPMI LSU1, ISPG, ISPH, cLIP1 (chloroplastic lipoate synthase 1), MIAB (methylthiotransferase), NIR, SIR, and THIC (4-amino-5-hydroxymethyl-2-methylpyrimidine phosphate synthase) and the [2Fe-2S]-containing SIRB (sirohydrochlorin ferrochelatase B). HCF101 was also included in the analysis as a positive control (Touraine *et al.*, 2019). The potential Fe-S client proteins cited above were assayed with NFU2 fused either to the binding (BD) or to the activation domain (AD) of the yeast GAL4 transcription factor. Because BD-NFU2, BD-HCF101 and AD-IPMI LSU1 showed transactivation capacities in the absence of 3-aminotriazol (3-AT) (Figure 5A), only yeast growth occurring in the presence of 2 mM 3-AT was considered as revealing positive interactions using these chimeric proteins. Doing so, 4 interactions were revealed with ASE2, IMPI LSU1 and cLIP1 in an AD-NFU2 configuration, and with ISPH in a BD-NFU2 configuration. This confirmed ASE2, IPMI LSU1 and ISPH, identified above either by LFQ proteomics or by Co-IP MS/MS as belonging to the NFU2 interacting network, and revealed cLIP1 as a new potential member of this network.

In order to get more insight into the specificity of these interactions, similar experiments were conducted with NFU3, the closest paralog of NFU2. NFU3 was found to interact with ISPH using both fusion proteins (Figures 5A and 5B), and with ASE2, cLIP1 and MIAB as an AD-

NFU3 fusion protein (Figure 5B). Altogether these results show that ASE2, ISPH and cLIP1 are potential clients shared by NFU2 and NFU3.

In planta analysis of NFU2 interactions with its novel putative targets by bimolecular fluorescence complementation (BiFC) assays

LFQ proteomic analysis of *nfu2-1* mutant together with Co-IP MS/MS experiments using NFU2:GFP fusion and Y2H directed screening yielded 14 proteins (*i.e.* APR2, ASE1, ASE2, DWARF27.2, FTR, GLU2, GLT1, IPMI LSU1, NDHI, NDHK, ISPG, ISPH, cLIP1 and PAO) for which no direct interaction or molecular connection with NFU2 was established in previous studies. The capacity of NFU2 to interact with these new potential targets was therefore assayed in plant cells using BiFC assays. For this purpose, all identified proteins were co-expressed as N-terminal fusions with either the N-terminal (protein-N fusions in figures) or the C-terminal (protein-C fusions in figures) region of the YFP protein in Arabidopsis protoplasts with either NFU2-C or NFU2-N, respectively.

Following Arabidopsis cell co-transfection, NFU2 could restore YFP fluorescence exclusively in chloroplasts when co-expressed with ASE1, ASE2, APR2, DWARF27.2, FTR, ISPG, ISPH, cLIP1 or PAO (Figure 6). These successful BiFCs were obtained independently of the fusion configuration (not shown), except with APR2 and DWARF27.2 for which the positive BiFC was obtained only in the NFU2-C configuration.

To evaluate overlapping interaction capacities of NFU isoforms, we also conducted BiFC experiments using NFU1 and NFU3. We identified several interactions involving NFU1 with APR2, ASE1, ASE2, FTR, ISPG, ISPH and cLIP1, and NFU3 with ASE1, FTR, ISPG, ISPH and cLIP1 (Figure S4). From these results, DWARF27.2 and PAO appear as the sole candidates specific to NFU2.

Altogether, these data highlight the interaction *in planta* between NFU2 and nine novel Fe-S proteins and indicate that most of these interactions are probably shared with NFU1 and/or NFU3.

DISCUSSION

Metabolic and physiological adjustments in the *nfu2* mutant

The proteins whose abundance was modified in the *nfu2-1* mutant compared to the WT were mostly cytosolic (roots and leaves) and chloroplastic (leaves and seedlings) (Figure 1). The majority of proteins whose abundance was decreased in *nfu2* was associated with the primary

metabolism (Figure 2). This is likely to adjust the metabolism in response to photosynthesis defects (Touraine *et al.*, 2004; Yabe *et al.*, 2004; Gao *et al.*, 2013). The most important variations in protein levels were found for PSI subunits, in accordance with previous studies highlighting important roles of NFU2, but also NFU3 and HCF101, in the establishment of a functional PSI (Touraine *et al.*, 2004; Yabe *et al.*, 2004; Gao *et al.*, 2013). The accumulation of specific PSI subunits (PsaA, B, C, D-1 and D-2) was already shown to be decreased in these mutants by WB. A clearer picture was obtained here as the LFQ proteomic approach showed that the abundance of 19 proteins (out of 31), which are part of PSI or involved in its assembly, was modified in the *nfu2-1* mutant, most of them being less accumulated (Table 1). Hence, the maturation defects of the Fe-S proteins, PsaA, PsaB and PsaC, whose abundance is strongly decreased in the *nfu2* mutant, have dramatic consequences on other subunits. This is consistent with previous studies showing that a defect in PsaE1 or in PsaD1/D2 affected the whole PSI, and notably the accumulation of PsaC and PsaD or PsaC and PsaE, respectively (Varotto *et al.*, 2000; Ihnatowicz *et al.*, 2004). The *psad* and *psae* mutants display growth and photosynthetic activity defects similar to those of *nfu2-1* mutants (Varotto *et al.*, 2000; Ihnatowicz *et al.*, 2004; Touraine *et al.*, 2019). It was also shown that the abundance of PsaF, G, H, L, N, O subunits as well as of Lhca-1 to 4 proteins was affected by the absence of PsaD (Ihnatowicz *et al.*, 2004). These observations indicate that the complex formed by these three proteins (PsaC, D and E1) on the stromal side of the PSI relies on a balanced stoichiometry between the three subunits.

A striking observation was that a large number of proteins related to the abiotic stress response have their abundance decreased in the *nfu2-1* mutant. In particular, several proteins were related to the response to desiccation in leaves of eight-week-old plants (Figure 3A). Consistently, the abscisic acid (ABA) content was about two-fold lower in *nfu2-1* mutant as compared with the WT and this was accompanied by a higher sensitivity to dehydration as assessed *via* rapid dehydration assays. This decrease implies that the biosynthesis and/or catabolism of this hormone are impaired. The synthesis of ABA relies on isoprenoid precursors (IPP and DMAPP), whose synthesis requires two Fe-S proteins in the non-mevalonate pathway (ISPG and ISPH), and then on derived carotenoids that are converted to ABA by several enzymatic reactions in plastids and in the cytosol (Finkelstein, 2013). One possibility could be that ISPG/H activities are altered in *nfu2-1* mutants, thus limiting the synthesis of ABA precursors such as carotenoids. However, global carotenoid levels are stable and zeaxanthin and antheraxanthin were shown to accumulate in *nfu2-1* mutants (Touraine *et al.*, 2004). Hence, a maturation defect should affect an Fe-S protein acting

downstream. The sole known Fe-S proteins that participate in the late-steps of ABA biosynthesis are the cytosolic abscisic aldehyde oxidases (AAO1-4) (Seo *et al.*, 2000). However, the assembly of Fe-S clusters in these AAOs should rely only on the cytosolic and mitochondrial Fe-S cluster assembly machineries but not on the SUF machinery. Moreover, their abundance does not vary in the *nfu2* mutant and most of the other proteins related to ABA biosynthesis or degradation were not quantifiable. It may actually be that one of the other enzymes involved in ABA synthesis has an Fe-S cluster, as not all of them have been biochemically characterized. Also, it is possible that rechanneling of ABA precursors towards the synthesis of more critical molecules occurs to sustain growth. Whether the loss of NFU2 function renders plants more susceptible to other abiotic stresses remains to be determined.

Identification of novel targets of NFU2

Among the 21 Fe-S proteins displaying an altered abundance in the *nfu2-1* mutant, as compared to the WT, 8 were previously analyzed by WB and/or by enzymatic activity measurements in the same genotypes. Overall, the comparison between these studies and the work presented here highlighted a good correlation. For instance, PsaA, B and C abundance was decreased in *nfu2-1* mutant leaves and seedlings as previously demonstrated by WB analyses (Touraine *et al.*, 2004; Yabe *et al.*, 2004; Hu *et al.*, 2017). Similarly, HCF101 decreased abundance in *nfu2-1* mutant leaves was in agreement with previous observations (Touraine *et al.*, 2019). Here, NIR and SIR accumulation was decreased only in *nfu2-1* mutant roots but not in seedlings or leaves. Similar observations were previously made by WB analysis but on whole plant tissues, most probably reflecting what was occurring in roots (Touraine *et al.*, 2004; Yabe *et al.*, 2004). However, a decrease of SIR activity in leaves was previously reported, indicating that the increased abundance of SIR observed in this study might correspond in part to the accumulation of apo-proteins (Touraine *et al.*, 2004). This latter observation may also indicate that a mechanism might exist in leaves to maintain SIR activity by increasing its protein level. Indeed, there is a single SIR gene in Arabidopsis that is essential for sulfur assimilation (Khan *et al.*, 2010). A similar observation was also made for FTR, which is consistent with the crucial role of FTR as a major actor for mediating the high demand of reducing power in leaves (but not in roots) to support the photosynthetic electron transport chain to several redox-sensitive target proteins (Schürmann & Buchanan, 2008; Yoshida *et al.*, 2019). GLU1 abundance was higher in *nfu2-1* mutant leaves and seedlings in accordance with a previous study reporting an increase of GLU activity in *nfu2-1* mutant plants (Touraine *et al.*, 2004). These results indicate that the loss of NFU2 function

activates some metabolic feedback stimulating the accumulation of GLU1 in aerial tissues and that it is likely that the transfer of Fe-S cluster to apo-GLU1 might occur independently of NFU2 *via* another Fe-S carrier protein. Conversely, the accumulation of FD (ferredoxin) was not in agreement with what was previously described by WB. For instance, it was shown that *nfu2* mutants displayed a lower level of FD accumulation compared to WT plants (Touraine *et al.*, 2004; Yabe *et al.*, 2004). This is in contrast to what was observed in this study as no variation was observed for FD2 (that represents 80% of the ferredoxin found in plants) in leaves, the sole tissue where this protein was detected and quantified. This discrepancy might be due to differences in the growth conditions between the studies but it cannot be excluded that some technical limitation comes from the LC-MS/MS analysis.

Based on the above-mentioned concordances between the results gathered in the literature and the data presented herein, it is likely that the 11 Fe-S proteins whose abundance was decreased in the *nfu2-1* mutant (*i.e.* APR2, ASE1, ASE2, DWARF27.2, FTR, GLU2, GLT1, IPMI LSU1, NDHK, NDHI and PAO) are true novel, direct or indirect, NFU2 clients. For those that cannot be validated by BiFC experiments in Arabidopsis protoplasts (GLU2, GLT1, IPMI LSU1, NDHK and NDHI), it is possible that the presence of YFP-tags prevented interactions in plant cells. Additionally, another intermediate Fe-S shuttle protein may act between NFU2 and these targets. This is for instance the case for PsaA, B and C proteins for which HCF101, which is abundant in green tissues, acts as an intermediate (Stockel & Oelmuller, 2004; Touraine *et al.*, 2019). In fact, the abundance of both HCF101 and these targets (GLU2, GLT1, NDHI and NDHK) are decreased in *nfu2-1* green tissues. In roots, HCF101 was neither detectable by LC-MS/MS nor by WB analyses. Hence, APR2, ASE1, ASE2, FTR, GLU2 and IPMI LSU1, whose abundance is decreased in this tissue, might be directly targeted by NFU2.

Three additional potential targets whose abundance was either not affected by the *nfu2-1* mutation (ISPG and ISPH) or not quantifiable in the interactomic experiments (cLIP1) have been identified. For these proteins, BiFC and Y2H experiments confirmed a direct interaction with NFU2. Hence, the lack of quantitative difference in protein abundance between *nfu2-1* and the WT for ISPG and ISPH suggests either that the apo-proteins are stable or that other transfer proteins than NFU2 promote their maturation. The validity of the connection between NFU2 and cLIP1 is reinforced by observations made in bacteria, yeast and human where the maturation of lipoate synthase depends on mitochondrial or cytosolic NFU counterparts (Navarro-Sastre *et al.*, 2011; Melber *et al.*, 2016; McCarthy & Booker, 2017).

More importantly, the expression of plastidial NFUs in the yeast *nfu1* mutant restored the defaults that were dependent on the lipoate synthase maturation defect (Uzarska *et al.*, 2018).

Partial overlap in Fe-S protein maturation among plastidial NFUs

Previous studies have highlighted that plastidial NFU2 and NFU3 proteins, but not NFU1, participate to the maturation of the same targets, either directly or through HCF101. This is best exemplified with NFU2 and NFU3 that both participate in the maturation of PsaA, B, C and possibly of DHAD in leaves (Nath *et al.*, 2016; Touraine *et al.*, 2019). Because the yeast complementation data mentioned above indicated that NFU1, NFU2 and NFU3 share common properties (Uzarska *et al.*, 2018), both NFU1 and NFU3 were included in BiFC experiments whereas only NFU3 was included in binary Y2H experiments as NFU1 was tested with the same proteins in another study (Roland *et al.*, 2020). Coupled with some previous studies, this allowed us to decrypt the overlap among plastidial NFUs in the maturation of Fe-S proteins (Figure 7). Overall, the results indicate that among novel Fe-S protein targets of NFU2, only few (*i.e.* five) seem specific. Unlike GLU2, GLT1 and SIR, the interactions with DWARF27.2 and PAO have been confirmed by BiFC and/or Y2H. Among other putative NFU2 targets, five (*i.e.* ASE2, FTR, ISPG, ISPH and cLIP1) were found to interact also with NFU1 and NFU3 and three are so far only shared with NFU1 (*i.e.* ASE1, APR2, IPMI LSU1). It is worth noting that no interactomic or quantitative proteomic experiment has been performed with NFU3, which could explain why there are globally less interactions described for this protein. In addition, NFU1 and NFU3 might also have specific partners, as Y2H experiments pointed to interactions between NFU1 and DWARF27.1 and THIC on the one hand and between NFU3 and MIAB on the other hand (Figures 5 and 7; Roland *et al.*, 2020).

In the future, it would be worth performing a similar exhaustive analysis with HCF101 because of its capacity to serve as a relay for NFU2 and NFU3. Also, assessing the capacity of all these NFU proteins to transfer their Fe-S clusters *in vitro* to their identified partners should be the priority of future works to unravel both efficiencies and constant rates of Fe-S transfer in NFU interaction networks. This is even more important as the novel Fe-S protein targets of NFU2 identified in this study contain different types of Fe-S clusters suggesting that in addition to transferring [4Fe-4S] and [2Fe-2S] clusters, NFU2 might transfer clusters of the [3Fe-4S] and [2Fe-2S]-Rieske types.

To conclude, this study brings new insights into the model of Fe-S protein maturation in plastids and highlights the potential role played by NFU2, but also by NFU1 and NFU3, in

the maturation of Fe-S proteins involved in diverse facets of the plant primary (*e.g.* photosynthesis, photorespiration, nitrogen and sulfur assimilation, purine and branched amino acid biosynthesis) and specialized (e.g. glucosinolate and isoprenoid biosynthesis) metabolisms (Figure 7). In depth metabolomic analyses of the respective single and double mutants grown in different conditions, when viable, may help deciphering which NFUs have a predominant role in a given physiological context.

ACKNOWLEGMENTS

This work was supported by the Agence Nationale de la Recherche as part of the 'Investissements d'Avenir' program (ANR-11-LABX-0002-01, Lab of Excellence ARBRE) and by grant no. ANR-2013-BSV6-0002-01 as well as by the Deutsche Forschungsgemeinschaft (DFG, INST 186/822-1) to IF. The PhD salary of M. Roland was provided by a funding from the Lorraine University of Excellence (LUE). All confocal analyses were performed on a device of the Montpellier Rio-Imaging and PHIV platform and benefited from assistance of C. Alcon. We thank M. Dauzat for help in preparing this manuscript.

1

REFERENCES

Abdel-Ghany SE, Ye H, Garifullina GF, Zhang L, Pilon-Smits EA, Pilon M. 2005. Iron-sulfur cluster biogenesis in chloroplasts. Involvement of the scaffold protein CpIscA. *Plant Physiology* **138**(1): 161-172.

Balk J, Pilon M. 2011. Ancient and essential: the assembly of iron-sulfur clusters in plants. *Trends in Plant Science* **16**(4): 218-226.

Balk J, Schaedler TA. 2014. Iron cofactor assembly in plants. *Annual Review of Plant Biology* **65**: 125-153.

Banci L, Brancaccio D, Ciofi-Baffoni S, Del Conte R, Gadepalli R, Mikolajczyk M, Neri S, Piccioli M, Winkelmann J. 2014. [2Fe-2S] cluster transfer in iron-sulfur protein biogenesis. *Proceeding of the National Academy of Sciences of the United States of America* **111**(17): 6203-6208.

Bandyopadhyay S, Gama F, Molina-Navarro MM, Gualberto JM, Claxton R, Naik SG, Huynh BH, Herrero E, Jacquot JP, Johnson MK, et al. 2008. Chloroplast monothiol glutaredoxins as scaffold proteins for the assembly and delivery of [2Fe-2S] clusters. *The EMBO Journal* **27**(7): 1122-1133.

Bradford MM. 1976. A rapid and sensitive method for the quantitation of microgram quantities of protein utilizing the principle of protein-dye binding. *Analytical Biochemistry* **72**: 248-254.

Brancaccio D, Gallo A, Mikolajczyk M, Zovo K, Palumaa P, Novellino E, Piccioli M, Ciofi-Baffoni S, Banci L. 2014. Formation of [4Fe-4S] clusters in the mitochondrial iron-sulfur cluster assembly machinery. *Journal of the American Chemical Society* **136**(46): 16240-16250.

Colin F, Martelli A, Clemancey M, Latour JM, Gambarelli S, Zeppieri L, Birck C, Page A, Puccio H, Ollagnier de Choudens S. 2013. Mammalian frataxin controls sulfur production and iron entry during de novo Fe4S4 cluster assembly. *Journal of the American Chemical Society* **135**(2): 733-740.

Couturier J, Wu HC, Dhalleine T, Pegeot H, Sudre D, Gualberto JM, Jacquot JP, Gaymard F, Vignols F, Rouhier N. 2014. Monothiol glutaredoxin-BolA interactions: redox control of Arabidopsis thaliana BolA2 and SufE1. *Molecular Plant* **7**(1): 187-205.

Couturier J, Touraine B, Briat JF, Gaymard F, Rouhier N. 2013. The iron-sulfur cluster assembly machineries in plants: current knowledge and open questions. *Frontiers in Plant Science* **4**: 259.

Cox J, Mann M. 2008. MaxQuant enables high peptide identification rates, individualized p.p.b.-range mass accuracies and proteome-wide protein quantification. *Nature Biotechnology* **26**(12): 1367-1372.

Cox J, Neuhauser N, Michalski A, Scheltema RA, Olsen JV, Mann M. 2011. Andromeda: a peptide search engine integrated into the MaxQuant environment. *Journal of Proteome Research* **10**(4): 1794-1805.

Finkelstein R. 2013. Abscisic Acid synthesis and response. *Arabidopsis Book* **11**: e0166.

Gao F, Robe K, Bettembourg M, Navarro N, Rofidal V, Santoni V, Gaymard F, Vignols F, Roschzttardtz H, Izquierdo E, et al. 2019. The Transcription Factor bHLH121 Interacts with bHLH105 (ILR3) and its Closest Homologs to Regulate Iron Homeostasis in Arabidopsis. *Plant Cell*. doi: 10.1105/tpc.19.00541.

Gao H, Azam T, Randeniya S, Couturier J, Rouhier N, Johnson MK. 2018. Function and maturation of the Fe-S center in dihydroxyacid dehydratase from Arabidopsis. The *Journal of Biological Chemistry* **293**(12): 4422-4433.

Gao H, Subramanian S, Couturier J, Naik SG, Kim SK, Leustek T, Knaff DB, Wu HC, Vignols F, Huynh BH, et al. 2013. Arabidopsis thaliana Nfu2 accommodates [2Fe-2S] or [4Fe-4S] clusters and is competent for in vitro maturation of chloroplast [2Fe-2S] and [4Fe-4S] cluster-containing proteins. *Biochemistry* **52**(38): 6633-6645.

Gervason S, Larkem D, Mansour AB, Botzanowski T, Muller CS, Pecqueur L, Le Pavec G, Delaunay-Moisan A, Brun O, Agramunt J, et al. 2019. Physiologically relevant

reconstitution of iron-sulfur cluster biosynthesis uncovers persulfide-processing functions of ferredoxin-2 and frataxin. *Nature Communications* **10**(1): 3566.

He Y, Chen B, Pang Q, Strul JM, Chen S. 2010. Functional specification of Arabidopsis isopropylmalate isomerases in glucosinolate and leucine biosynthesis. *Plant and Cell Physiology* **51**(9): 1480-1487.

Herrfurth C, Feussner I. 2020. Quantitative Jasmonate Profiling Using a High-Throughput UPLC-NanoESI-MS/MS Method. In: A. Champion L. Laplaze eds. Jasmonate in Plant Biology: Methods and Protocols. New York, NY: Springer US, 169-187.

Holscher C, Lutterbey MC, Lansing H, Meyer T, Fischer K, von Schaewen A. 2016. Defects in Peroxisomal 6-Phosphogluconate Dehydrogenase Isoform PGD2 Prevent Gametophytic Interaction in Arabidopsis thaliana. *Plant Physiology* **171**(1): 192-205.

Hooper CM, Castleden I, Tanz SK, Aryamanesh, and Millar, AH. 2017. SUBA4: the interactive data analysis centre for Arabidopsis subcellular protein locations *Nucleic Acids Research* **45**(D1):D1064-D1074.

Hu X, Kato Y, Sumida A, Tanaka A, Tanaka R. 2017. The SUFBC2 D complex is required for the biogenesis of all major classes of plastid Fe-S proteins. *The Plant Journal* **90**(2): 235-248.

Ihnatowicz A, Pesaresi P, Varotto C, Richly E, Schneider A, Jahns P, Salamini F, Leister D. 2004. Mutants for photosystem I subunit D of Arabidopsis thaliana: effects on photosynthesis, photosystem I stability and expression of nuclear genes for chloroplast functions. *The Plant Journal* **37**(6): 839-852.

Juhnke H, Krems B, Kotter P, Entian KD. 1996. Mutants that show increased sensitivity to hydrogen peroxide reveal an important role for the pentose phosphate pathway in protection of yeast against oxidative stress. *Molecular GeneralGenetics* **252**(4): 456-464.

Khan MS, Haas FH, Samami AA, Gholami AM, Bauer A, Fellenberg K, Reichelt M, Hänsch R, Mendel RR, Meyer AJ, Wirtz M, Hell R. 2010. Sulfite reductase defines

a newly discovered bottleneck for assimilatory sulfate reduction and is essential for growth and development in Arabidopsis thaliana. *The Plant Cell* **22**(4): 1216-1231.

Knill T, Reichelt M, Paetz C, Gershenzon J, Binder S. 2009. Arabidopsis thaliana encodes a bacterial-type heterodimeric isopropylmalate isomerase involved in both Leu biosynthesis and the Met chain elongation pathway of glucosinolate formation. *Plant Molecular Biology* **71**(3): 227-239.

Lachler K, Imhof J, Reichelt M, Gershenzon J, Binder S. 2015. The cytosolic branched-chain aminotransferases of Arabidopsis thaliana influence methionine supply, salvage and glucosinolate metabolism. *Plant Molecular Biology* **88**(1-2): 119-131.

Laemmli UK. 1970. Cleavage of structural proteins during the assembly of the head of bacteriophage T4. *Nature* **227**(5259): 680-685.

Lezhneva L, Meurer J. 2004. The nuclear factor HCF145 affects chloroplast psaA-psaB-rps14 transcript abundance in Arabidopsis thaliana. *The Plant Journal* **38**(5): 740-753.

Lichtenthaler FW. 1987. Karl Freudenberg, Burckhardt Helferich, Hermann O. L. Fischer: a centennial tribute. *Carbohydrate Research* **164**: 1-22.

Mapolelo DT, Zhang B, Randeniya S, Albetel AN, Li H, Couturier J, Outten CE, Rouhier N, Johnson MK. 2013. Monothiol glutaredoxins and A-type proteins: partners in Fe-S cluster trafficking. *Dalton Transactions* **42**(9): 3107-3115.

McCarthy EL, Booker SJ. 2017. Destruction and reformation of an iron-sulfur cluster during catalysis by lipoyl synthase. *Science* **358**(6361): 373-377.

Melber A, Na U, Vashisht A, Weiler BD, Lill R, Wohlschlegel JA, Winge DR. 2016. Role of Nfu1 and Bol3 in iron-sulfur cluster transfer to mitochondrial clients. *Elife* **5**.

Mueller C, Schwender J, Zeidler J, Lichtenthaler HK. 2000. Properties and inhibition of the first two enzymes of the non-mevalonate pathway of isoprenoid biosynthesis. *Biochemical Society Transactions* **28**(6): 792-793.

Nakagawa T, Suzuki T, Murata S, Nakamura S, Hino T, Maeo K, Tabata R, Kawai T, Tanaka K, Niwa Y, et al. 2007. Improved Gateway binary vectors: high-performance

vectors for creation of fusion constructs in transgenic analysis of plants. *Biosci Biotechnology and applied Biochemistry* **71**(8): 2095-2100.

Nath K, Wessendorf RL, Lu Y. 2016. A Nitrogen-Fixing Subunit Essential for Accumulating 4Fe-4S-Containing Photosystem I Core Proteins. *Plant Physiology* **172**(4): 2459-2470.

Navarro-Sastre A, Tort F, Stehling O, Uzarska MA, Arranz JA, Del Toro M, Labayru MT, Landa J, Font A, Garcia-Villoria J, et al. 2011. A fatal mitochondrial disease is associated with defective NFU1 function in the maturation of a subset of mitochondrial Fe-S proteins. *The American Journal Human Genetics* **89**(5): 656-667.

North HM, Frey A, Boutin JP, Sotta B, Marion-Poll A. 2005. Analysis of xanthophyll cycle gene expression during the adaptation of Arabidopsis to excess light and drought stress: Changes in RNA steady-state levels do not contribute to short-term responses. *Plant Science* **169**(1): 115-124.

Pilon M, Abdel-Ghany SE, Van Hoewyk D, Ye H, Pilon-Smits EA. 2006. Biogenesis of iron-sulfur cluster proteins in plastids. *Genetic Engineering (N Y)* **27**: 101-117.

Przybyla-Toscano J, Roland M, Gaymard F, Couturier J, Rouhier N. 2018. Roles and maturation of iron-sulfur proteins in plastids. *Journal of Biological Inorgarnic Chemistry* **23**(4): 545-566.

Rey P, Becuwe N, Tourrette S, Rouhier N. 2017. Involvement of Arabidopsis glutaredoxin S14 in the maintenance of chlorophyll content. *Plant Cell and Environment* **40**(10): 2319-2332.

Roland M, Przybyla-Toscano J, Vignols F, Berger N, Azam T, Christ L, Santoni V, Wu H-C, Dhalleine T, Johnson MK, Dubos C, Couturier J, Rouhier N. 2020. The plastidial Arabidopsis thaliana NFU1 protein binds and delivers [4Fe-4S] clusters to specific client proteins. *The Journal of Biological. Chemistry* 295(6): 1727-1742

Rowland E, Kim J, Bhuiyan NH, van Wijk KJ. 2015. The Arabidopsis Chloroplast Stromal N-Terminome: Complexities of Amino-Terminal Protein Maturation and Stability. *Plant Physiology* **169**(3): 1881-1896.

Sawada Y, Kuwahara A, Nagano M, Narisawa T, Sakata A, Saito K, Hirai MY. 2009. Omics-based approaches to methionine side chain elongation in Arabidopsis: characterization of the genes encoding methylthioalkylmalate isomerase and methylthioalkylmalate dehydrogenase. *Plant and Cell Physiology* **50**(7): 1181-1190.

Schürmann P, Buchanan BB. 2008. The ferredoxin/thioredoxin system of oxygenic photosynthesis. *Antioxidants and Redox Signaling* **10**(7): 1235-74.

Seo M, Peeters AJ, Koiwai H, Oritani T, Marion-Poll A, Zeevaart JA, Koornneef M, Kamiya Y, Koshiba T. 2000. The Arabidopsis aldehyde oxidase 3 (AAO3) gene product catalyzes the final step in abscisic acid biosynthesis in leaves. *Proceeding of the National Academy of Sciences of the United States of America* **97**(23): 12908-12913.

Stincone A, Prigione A, Cramer T, Wamelink MM, Campbell K, Cheung E, Olin-Sandoval V, Gruning NM, Kruger A, Tauqeer Alam M, et al. 2015. The return of metabolism: biochemistry and physiology of the pentose phosphate pathway. *Biological Review of Cambridge Philosophical Society* **90**(3): 927-963.

Stockel J, Oelmuller R. 2004. A novel protein for photosystem I biogenesis. *The Journal of Biological Chemistry* **279**(11): 10243-10251.

Touraine B, Boutin JP, Marion-Poll A, Briat JF, Peltier G, Lobreaux S. 2004. Nfu2: a scaffold protein required for [4Fe-4S] and ferredoxin iron-sulphur cluster assembly in Arabidopsis chloroplasts. *The Plant Journal* **40**(1): 101-111.

Touraine B, Vignols F, Przybyla-Toscano J, Ischebeck T, Dhalleine T, Wu HC, Magno C, Berger N, Couturier J, Dubos C, et al. 2019. Iron-sulfur protein NFU2 is required for branched-chain amino acid synthesis in Arabidopsis roots. *Journal of Experimental Botany* **70**(6): 1875-1889.

Uzarska MA, Przybyla-Toscano J, Spantgar F, Zannini F, Lill R, Muhlenhoff U, Rouhier N. 2018. Conserved functions of Arabidopsis mitochondrial late-acting maturation factors in the trafficking of ironsulfur clusters. *Biochimica et Biophysica Acta Molecular Cell Research* **1865**(9): 1250-1259.

Varotto C, Pesaresi P, Meurer J, Oelmuller R, Steiner-Lange S, Salamini F, Leister D. 2000. Disruption of the Arabidopsis photosystem I gene psaE1 affects photosynthesis and impairs growth. *The Plant Journal* **22**(2): 115-124.

Vignols F, Brehelin C, Surdin-Kerjan Y, Thomas D, Meyer Y. 2005. A yeast two-hybrid knockout strain to explore thioredoxin-interacting proteins in vivo. *Proceeding of the National Academy of Sciences of the United States of America* **102**(46): 16729-16734.

Walter M, Chaban C, Schutze K, Batistic O, Weckermann K, Nake C, Blazevic D, Grefen C, Schumacher K, Oecking C, et al. 2004. Visualization of protein interactions in living plant cells using bimolecular fluorescence complementation. *The Plant Journal* **40**(3): 428-438.

Yabe T, Morimoto K, Kikuchi S, Nishio K, Terashima I, Nakai M. 2004. The Arabidopsis chloroplastic NifU-like protein CnfU, which can act as an iron-sulfur cluster scaffold protein, is required for biogenesis of ferredoxin and photosystem I. *The Plant Cell* **16**(4): 993-1007.

Yabe T, Nakai M. 2006. Arabidopsis AtIscA-I is affected by deficiency of Fe-S cluster biosynthetic scaffold AtCnfU-V. *Biochemical and Biophysical Resarch Communications* **340**(4): 1047-1052.

Yoo SD, Cho YH, Sheen J. 2007. Arabidopsis mesophyll protoplasts: a versatile cell system for transient gene expression analysis. *Nature Protocols* **2**(7): 1565-1572.

Yoshida K, Yokochi Y, Hisabori T. 2019. New Light on Chloroplast Redox Regulation: Molecular Mechanism of Protein Thiol Oxidation. *Frontiers in Plant Science* **10**:1534.

Table 1. Abundance of photosystem I associated proteins in *nfu2-1* relative to wild type.
n.q.: not quantifiable, n.v.: no variation, n.d.: not detected.

ID	Acronym	log2 (FC) leaves	log2 (FC) seedlings	Function	Name
AtCg00350	PsaA	**-1.09***	**-1.68****	PSI core	Photosystem I subunit A
AtCg00340	PsaB	**1.01***	**-1.81****	PSI core	Photosystem I subunit B
AtCg01060	PsaC	**-1.15****	**-2.10****	PSI core	Photosystem I subunit C
At1g31330	PsaF	**-0.89***	**-2.05***	PSI core	Photosystem I subunit F
At1g55670	PsaG	**-1.32***	**-1.58****	PSI core	Photosystem I subunit G
At3g16140	PsaH-1	n.v.	n.d.	PSI core	Photosystem I subunit H-1
At1g52230	PsaH-2	**-0.94****	**-2.50****	PSI core	Photosystem I subunit H-2
AtCg00510	PsaI	n.v.	n.d.	PSI core	Photosystem I subunit I
AtCg00630	PsaJ	n.v.	n.q.	PSI core	Photosystem I subunit J
At1g30380	PsaK	**-1.06****	**-1.64****	PSI core	Photosystem I subunit K
At4g12800	PsaL	n.v.	**-1.77****	PSI core	Photosystem I subunit L
At1g08380	Psa0	n.v.	**-1.98****	PSI core	Photosystem I subunit O
At4g02770	PsaD-1	**-0.80****	n.d.	PSI peripheral	Photosystem I subunit D-1
At1g03130	PsaD-2	**-0.86****	**-1.92****	PSI peripheral	Photosystem I subunit D-2
At4g28750	PsaE-1	**-0.76****	**-2.01****	PSI peripheral	Photosystem I subunit E-1
At2g20260	PsaE-2	n.v.	**-1.00****	PSI peripheral	Photosystem I subunit E-2
At5g64040	PsaN	**-0.86****	**-2.13****	PSI peripheral	Photosystem I subunit N
At2g46820	PsaP	n.v.	n.v.	PSI peripheral	Photosystem I subunit P
At3g54890	Lhca-1	**-0.30***	**-0.41***	PSI antenna	Photosystem I light harvesting complex gene 1
At3g61470	Lhca-2	**-0.71****	**-1.00****	PSI antenna	Photosystem I light harvesting complex gene 2
At1g61520	Lhca-3	**-0.53****	**-1.13****	PSI antenna	Photosystem I light harvesting complex gene 3
At3g47470	Lhca-4	n.v.	**-0.49****	PSI antenna	Photosystem I light harvesting complex gene 4
At1g45474	Lhca-5	n.v.	**-2.02***	PSI antenna	Photosystem I light harvesting complex gene 5
At1g19150	Lhca-6	**+0.29***	n.v.	PSI antenna	Photosystem I light harvesting complex gene 6
At2g44860	PSA2	n.q.	n.d.	PSI	Photosystem I assemby 2

				chaperone	
At3g55250	PSA3	n.v.	n.v.	PSI chaperone	Photosystem I assemby 3
AtCg00360	Ycf3	n.q.	**+0.27***	PSI chaperone	Hypothetical chloroplast open reading frame 3
AtCg00520	Ycf4	n.v.	n.q.	PSI chaperone	Hypothetical chloroplast open reading frame 4
At1g22700	PYG7	**+0.54****	**+0.49***	PSI chaperone	Pale yellow green 7
At5g44650	Y3IP1	n.v.	**-0.35****	PSI chaperone	YCF3-interacting protein 1
At4g15510	PPD1	**+0.43***	n.v.	PSI chaperone	PsbP domain protein 1

Table 2. Abundance of chloroplastic Fe-S proteins in *nfu2-1* relative to wild type. n.q.: not quantifiable, n.v.: no variation, n.d.: not detected, absent: not detected in *nfu2-1* mutant, #: Fe-S cluster identified in algae but not confirmed in plants. No variation was measured for the following chloroplastic proteins: APR1 and APR3 (Adenosine 5'-phosphosulfate reductase 1 and 3), ASE3 (Amidophosphoribosyltransferase 3), CAO (Chlorophyll a oxygenase), CDJ1, 2 and 3 (DNA J protein C77, C76 and C82), CMO (putative choline monooxygenase), DWARF27.1 and 3, FD1 (PETF2), 2 (PETF), 3 and 4 (Ferredoxin 1, 2, 3 and 4), HCAR (7-hydroxymethyl chlorophyll a reductase), IPMSI (Isopropylmalate synthase), ISPG (4-Hydroxy-2-methylbut-2-enyl diphosphate synthase), ISPH (4-Hydroxy-2-methylbut-2-enyl), cLIP1 (Lipoyl synthase 1), MIAB (Methylthiotransferase), NFU1, 2 and 3 (NFU domain protein 1, 2 and 3), PetC (Photosynthetic electron transfer C), PTC52 (Protochlorophyllide-dependent translocon component 52), SIRB (Sirohydrochlorin ferrochelatase B), SUFA1, SUFB, SUFE3, THIC (4-amino-5-hydroxymethyl-2-methylpyrimidine phosphate synthase) and TIC55 (Translocon at the inner envelope membrane of chloroplast 55).

ID	Acronym	log2 (FC) roots	log2 (FC) leaves	log2 (FC) seedlings	Fe-S cluster	Function	Name
At1g62180	APR2	**absent**	n.v.	n.q.	[4Fe-4S]	Sulfate assimilation	Adenosine 5'-phosphosulfate reductase 2
At2g16570	ASE1	**-0.26***	n.v.	n.q.	[4Fe-4S]	Purine nucleotide biosynthesis	Amidophosphoribosyltransferase 1
At4g34740	ASE2	**-0.44****	n.v.	n.v.	[4Fe-4S]	Purine nucleotide biosynthesis	Amidophosphoribosyltransferase 2
At3g23940	DHAD	**-0.11***	n.v.	n.v.	[2Fe-2S]	Branched chain amino acid biosynthesis	Dihydroxyacid dehydratase
At1g64680	DWARF 27.2	n.d.	**-0.88****	n.q.	[4Fe-4S] (?)	Unknown	DWARF27.2
At2g04700	FTR	**-0.75***	**+0.33***	**+0.31****	[4Fe-4S]	Ferredoxin-thioredoxin reductase	Ferredoxin-thioredoxin reductase
At3g24430	HCF101	n.d.	**-0.32***	n.v.	[4Fe-4S]	Fe-S cluster transfer	High chlorophyll fluorescence 101
At5g04140	**GLU1**	n.q.	**+0.45****	**+0.83****	[3Fe-4S]	Nitrate assimilation	Glutamate synthase 1 (Fd-GOGAT)
At2g41220	GLU2	**-0.55***	**-0.33***	n.q.	[3Fe-4S]	Nitrate assimilation	Glutamate synthase 2 (Fd-GOGAT)
At5g53460	**GLT1**	n.v.	n.v.	**-0.60****	[3Fe-4S]	Nitrate assimilation	Glutamate synthase 1 (NADH-dependent)

At4g13430	IPMI LSU1	**-0.56***	n.v.	n.v.	[4Fe-4S]	Leucine biosynthesis	Isopropylmalate isomerase (large subunit 1)
AtCg00430	NDHK	n.d.	**-0.29***	n.v.	[4Fe-4S]	Aerobic respiration	NADH dehydrogenase (subunit K)
AtCg01090	NDHI	n.d.	**-0.42****	n.v.	2x [4Fe-4S]	Photosynthesis	NADPH dehydrogenase (subunit I)
At5g51720	NEET	n.d.	**+0.37***	n.v.	[2Fe-2S]	Iron homeostasis	NEET
At2g15620	NIR	**-0.64****	n.v.	n.v.	[4Fe-4S]	Nitrate assimilation	Nitrite reductase
At3g44880	PAO	n.d.	n.v.	**-0.25***	rieske [2Fe-2S]	Chlorophyll catabolism	Pheophorbide a oxygenase
AtCg00350	PsaA	n.d.	**-1.09***	**-1.68****	[4Fe-4S]	Photosynthesis	PsaA subunit of photosystem I
AtCg00340	PsaB	n.d.	**-1.01***	**-1.81****	[4Fe-4S]	Photosynthesis	PsaB subunit of photosystem I
AtCg01060	PsaC	n.d.	**-1.14****	**-2.02****	[4Fe-4S]	Photosynthesis	PsaC subunit of photosystem I
At1g71500	PSB33	n.d.	**+0.30***	**+0.45****	[2Fe-2S] #	Photosynthesis	Photosystem B protein 33
At5g04590	SIR	**-0.37****	**+0.31***	n.v.	[4Fe-4S]	Sulfate assimilation	Sulfite reductase

Table 3. NFU2-interacting chloroplastic proteins identified by Co-IP. n.q.: not quantified.

Gene ID	mean_intensity *Pro35S:CTP$_{NFU3}$GFP*	mean_intensity *Pro35S:NFU2:GFP*	Log2 (FC)	Acronym	Name	Function	Localisation	Fe-S cluster type
AT5G53460	16.18	19.96	3.78	GLT1	NADH-dependent glutamate synthase 1	Glutamate biosynthesis	Chloroplast	[3Fe-4S]
AT5G04140	19.33	21.03	1.70	GLU1	Glutamate synthase 1	Glutamate biosynthesis	Chloroplast Mitochondria	[3Fe-4S]
AT4G34350	n.q.	21.63	Absent	ISPH	4-hydroxy-3-methylbut-2-enyl diphosphate reductase	Chlorophyll & carotenoid biosynthesis	Chloroplast	[4Fe-4S]
AT5G60600	n.q.	20.76	Absent	ISPG	4-hydroxy-3-methylbut-2-enyl diphosphate synthase	Chlorophyll & carotenoid biosynthesis	Chloroplast	[3Fe-4S]
AT4G27440	20.26	24.08	3.82	PORB	Protochlorophyllide oxidoreductase B	Chlorophyll biosynthesis	Chloroplast	None
AT5G30510	18.55	21.81	3.26	RPS1	Ribosomal protein S1	Plastid translation machinery	Chloroplast	None
AT4G13670	18.41	21.42	3.01	PTAC5	Plastid transcriptionally active 5	Chloroplast development	Chloroplast	None
AT3G62030	21.14	23.69	2.56	ROC4	Rotamase CYP 4	PSII stability and repair	Chloroplast (stroma)	None
AT2G04030	20.44	22.85	2.41	Hsp88.1	Chaperone protein htpG family protein	Protein import	Chloroplast (stroma)	None
AT3G12780	24.55	26.76	2.21	PGK1	Phosphoglycerate kinase 1	Calvin cycle	Chloroplast (stroma)	None
AT4G20360	24.25	26.33	2.08	ATRAB	RAB GTPase	Unknown	Chloroplast	None

				E1B	homolog E1B			
AT5G52920	18.83	20.81	1.98	PKP1	Plastidic pyruvate kinase beta subunit 1	Fatty acid biosynthesis	Chloroplast	None
AT3G14415	21.40	23.34	1.94	GOX2	Glyoxylate oxidase	Photorespiration	Peroxisome	None
ATCG00720	19.21	21.01	1.80	PETB	Photosynthetic electron transfer B	Cytochrome b6f	Chloroplast (thylakoid)	None
AT3G52150	19.36	20.95	1.59	PSRP2	Plastid specific ribosomal protein 2	Plastid translation machinery	Chloroplast	None
AT2G39730	24.41	25.97	1.55	RCA	Rubisco activase	Carbon assimilation	Chloroplast	None
AT2G38540	19.96	21.41	1.45	LTP1	Lipid transfer protein 1	Pathogen response	Chloroplast (thylakoid) Cell wall	None
AT3G50820	19.28	20.69	1.42	PSBO2,	Photosystem II subunit O-2	PSII	Chloroplast	None
AT4G21280	21.43	22.83	1.40	PSBQA	Photosystem II subunit QA	PSII	Chloroplast	None
AT4G10340	22.85	24.21	1.36	LHCB5	Light harvesting complex of photosystem II 5	PSII	Chloroplast	None
AT4G27090	19.15	20.34	1.19		Ribosomal protein L14	Plastid translation machinery	Chloroplast	None
AT5G45390	21.62	22.31	0.69	CLPP4	CLP protease P4	Protein quality control	Chloroplast	None
AT4G30620	n.q.	19.04	Absent	STCL	STIC2 like	Protein import	Chloroplast	None
AT2G27820	n.q.	19.34	Absent	PD1	Prephenate dehydratase 1	Phenylalanine & tyrosine biosynthesis	Chloroplast	None

AT5G45930	n.q.	21.46	Absent	CHLI2	Magnesium chelatase i2	Chlorophyll biosynthesis	Chloroplast	None
AT5G67030	n.q.	17.08	Absent	ABA1	Zeaxanthin epoxidase	ABA biosynthesis	Chloroplast	None

FIGURE LEGENDS

Figure 1. *Subcellular localization of proteins whose abundance is significantly affected by the *nfu2-1* mutation.*

Proteins were extracted from *Arabidopsis thaliana* roots **(A)**, leaves **(B)** and seedlings **(C)**. Protein localization was analyzed *in silico* using the multiple marker abundance profiling method of the SUBA4 bioinformatic platform (http://suba.live/).

Figure 2. Gene ontology (GO) analysis of proteins whose abundance is significantly affected by the *nfu2-1* mutation.

Proteins were extracted from *Arabidopsis thaliana* roots **(A)**, leaves **(B)** and seedlings **(C)**. GO term enrichment analysis was conducted using the PANTHER gene ontology platform (http://go.pantherdb.org). This figure is available in colour at JXB online.

Figure 3. *nfu2-1* mutation affects the plant response to dehydration.

(A) Variation in the quantitative protein abundance of dehydration response marker proteins in *nfu2-1 vs* WT plants expressed in log2 Fold Change. ALDH7B4, aldehyde dehydrogenase 7B4; RD29A, response to desiccation 29A; RD2, response to desiccation 2; LEA14, late embryogenesis abundant 14; PIP2;3, plasma membrane intrinsic protein 2;3, ERD14, early response to dehydration 14; P5SCA, delta 1-pyrroline-5-carboxylate synthase; PXG3, peroxygenase 3. **(B)** ABA content in WT and *nfu2-1* seedlings. **(C)** Rapid dehydration assay conducted on detached WT and *nfu2-1* leaves. **(B-C)** n = 3 biological repeats. Error bars show ± SD. *t*-test significant difference: ***, $p < 0.001$. This figure is available in colour at JXB online.

Figure 4. Effect of fosmidomycin treatment on wild type and *nfu2-1* seedlings.

Fosmidomycin is an inhibitor of the biogenesis of IPP (isopentenyl diphosphate) and DMAPP (dimethylallyl diphosphate), the precursors for the biosynthesis of isoprenoids and their derived molecules (e.g. chlorophylls, carotenoids, ABA). Dose-dependent effect of fosmidomycin on chlorophyll content **(A)**, carotenoid content **(B)**, fresh weight **(C)** and root length **(D)** of *Arabidopsis thaliana* WT and *nfu2-1* seedlings. **(A-D)** Means within each condition with the same letter are not significantly different according to one-way ANOVA followed by post-hoc Tukey test, $p < 0.05$ (n = 3 technical repeats from one representative experiment). Error bars show ± SD. This figure is available in colour at JXB online.

Figure 5. Binary yeast two-hybrid interaction screen between plastidial NFU2 or NFU3 and selected Fe-S-containing proteins.

Control plates contained histidine (+His) and test plates were without histidine (–His) in the absence or presence (2 mM) of 3-aminotriazol (+3AT). The images shown are representative of three independent transformation experiments. Constructs expressing NFUs (NFU2 and NFU3) are fused either to the Gal4 DNA-binding domain (BD, NFUs used as baits) **(A)** or to the Gal4 activator domain (AD, NFUs used as preys) **(B)**. This figure is available in colour at JXB online.

Figure 6. Bimolecular fluorescence complementation assays between NFU2 and potential novel Fe-S client proteins identified in this study.

NFU2 fused upstream of the YFP C-terminal region (NFU2-C, left in panels) was co-expressed with each of its potential Fe-S protein target fused upstream of the YFP N-terminal region (protein-N, left in panels) in *Arabidopsis thaliana* protoplasts. The YFP fluorescence was recorded 24h post-transfection by confocal microscopy. All these positive BiFCs were also observed when Protein-C / NFU2-N configurations were used (not shown) except for DWARF27.2-C / NFU2-N pairwise that did not allow fluorescence reconstitution. All confocal images were recorded without the need of a maximum Z-stack intensity projection. All negative controls verifying that none of the proteins tested alone with the empty partner vector can restore YFP fluorescence are given in Figure S4 (for client Fe-S proteins) and in Touraine *et al.*, 2019 (for NFU2). YFP, yellow fluorescent protein; Chl, chlorophyll fluorescence. Bars = 10 µm.

Figure 7. Summary scheme integrating known and newly identified NFU2 client proteins and redundancy with its NFU1 and NFU3 paralogs.

Among the 24 NFU2 client proteins, 14 were newly identified in this study by combining three different approaches: label free quantitative proteomic (LFQ) analysis using the *nfu2-1* loss-of-function mutant, protein interactomics using a NFU2:GFP fusion as bait and binary interaction screen in yeast (Y2H) using NFU2 (as well as NFU3) and selected Fe-S proteins. The interactions between these 14 Fe-S proteins and NFU2, as well as NFU1 and NFU3, were then tested by bimolecular fluorescence complementation (BiFC) assays. N: Novel NFU2 targets identified in this study, P: NFU2 targets identified in this study by LFQ proteomic analysis, I: NFU2 targets identified in this study by interactomics. *: NFU3 interaction with ASE2 was seen only in Y2H.

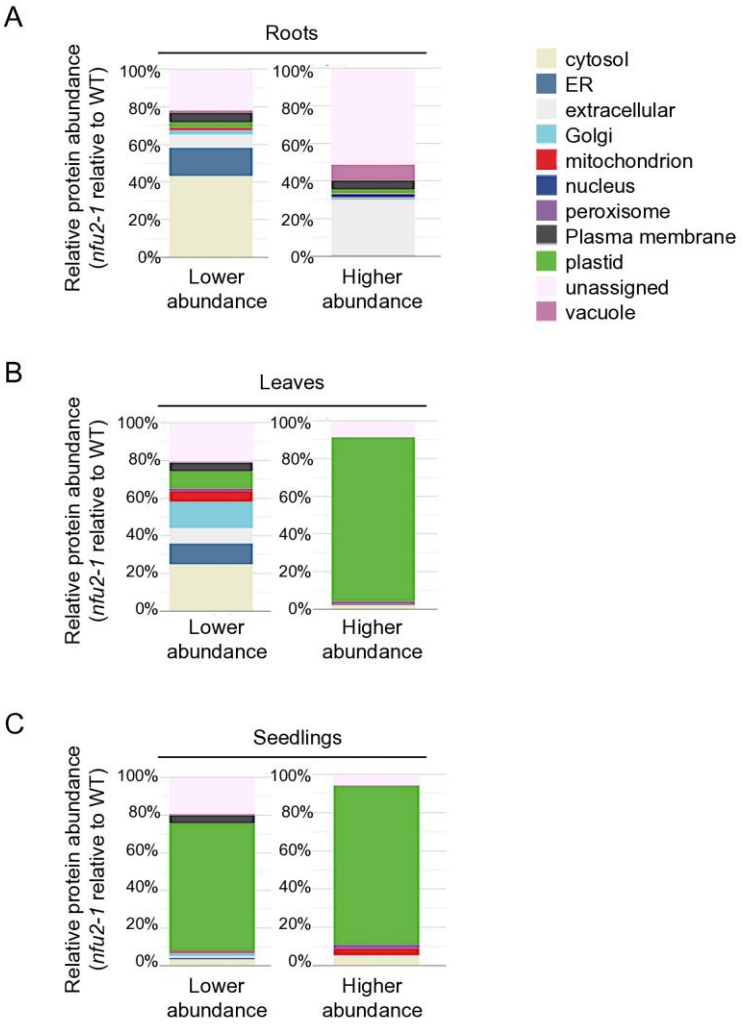

Figure 1. *Subcellular localization of proteins whose abundance was significantly affected by the nfu2-1* mutation. Proteins were extracted from *Arabidopsis thaliana* **(A)** roots, **(B)** leaves and **(C)** seedlings. Protein localization was analyzed *in silico* using the multiple marker abundance profiling method of the SUBA4 bioinformatic platform (http://suba.live/).

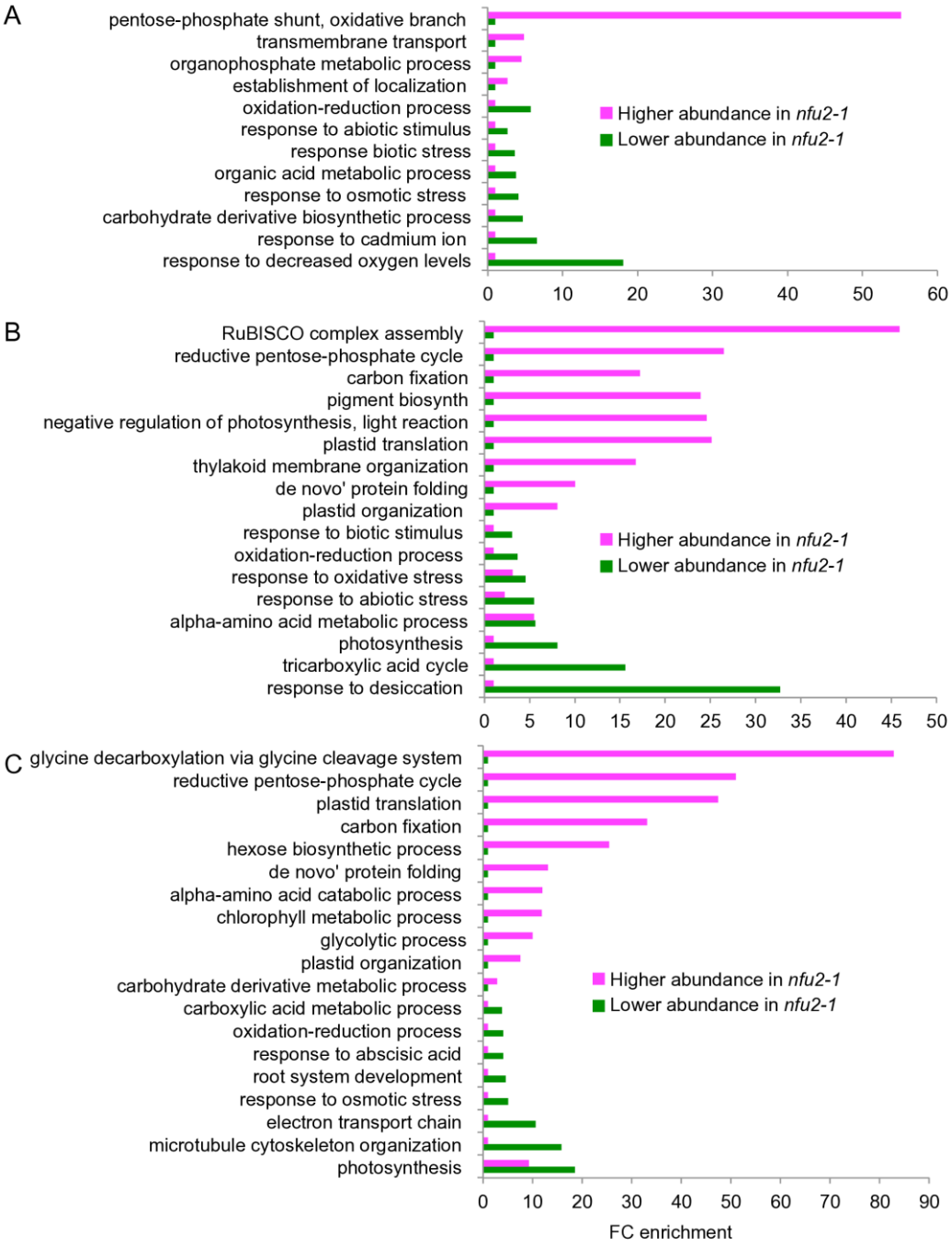

Figure 2. Gene ontology (GO) analysis of proteins whose abundance was significantly affected by the *nfu2-1* mutation. Proteins were extracted from *Arabidopsis thaliana* **(A)** roots, **(B)** leaves and **(C)** seedlings. GO term enrichment analysis was conducted using the PANTHER gene ontology platform (http://go.pantherdb.org). This figure is available in colour at JXB online.

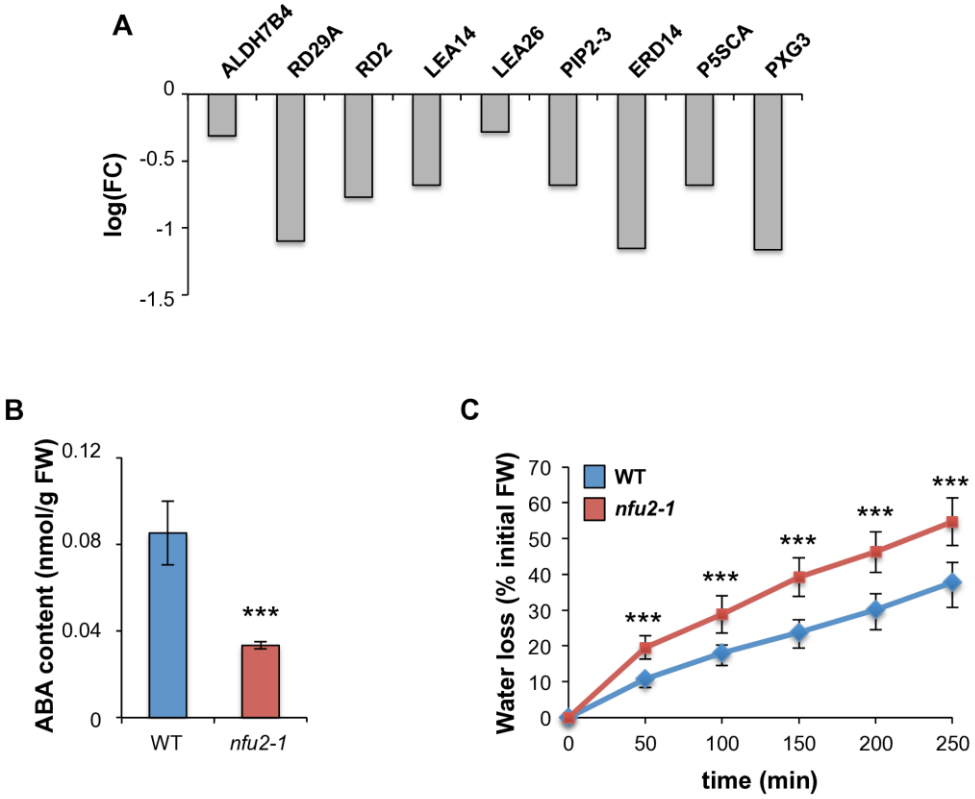

Figure 3. *nfu2-1* mutation affects the plant response to dehydration. (A) Protein abundance in *nfu2-1* in comparison to the wild type (log Fold Change) of dehydration response marker proteins (ALDH7B4, aldehyde dehydrogenase 7B4; RD29A, response to desiccation 29A; RD2, response to desiccation 2; LEA14, late embryogenesis abundant 14; PIP2;3, plasma membrane intrinsic protein 2;3, ERD14, early response to dehydration 14; P5SCA, delta 1-pyrroline-5-carboxylate synthase; PXG3, peroxygenase 3). **(B)** ABA content in wild type and *nfu2-1* seedlings. **(C)** Rapid dehydration assay conducted on detached wild type and nfu2-1 leaves. **(B-C)** n = 3 biological repeats. Error bars show ±SD. *t*-test significant difference: ***, $p < 0.001$. This figure is available in colour at JXB online.

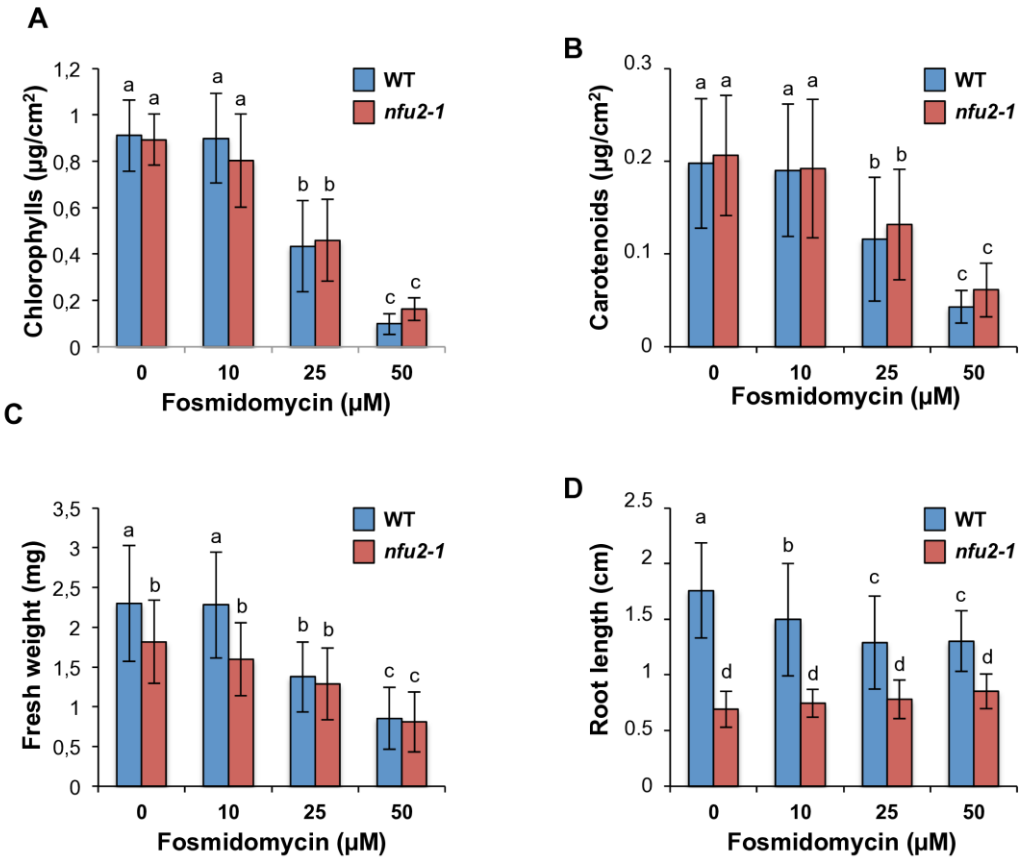

Figure 4. Effect of fosmidomycin treatment on wild type (WT) and *nfu2-1* seedlings.
Fosmidomycin is an inhibitor of the biogenesis of IPP (isopentenyl diphosphate) and DMAPP (dimethylallyl diphosphate), the precursors for the biosynthesis of isoprenoids (e.g chlorophylls, carotenoid, ABA). Dose dependent effect of fosmidomycin on **(A)** chlorophylls content, **(B)** carotenoids content, **(C)** fresh weight and **(D)** root length of *Arabidopsis thaliana* WT and *nfu2-1* seedlings. **(A-D)** Means within each condition with the same letter are not significantly different according to one-way ANOVA followed by post-hoc Tukey test, $p < 0.05$ (n = 3 technical repeats from one representative experiment). Error bars show ±SD. This figure is available in colour at JXB online.

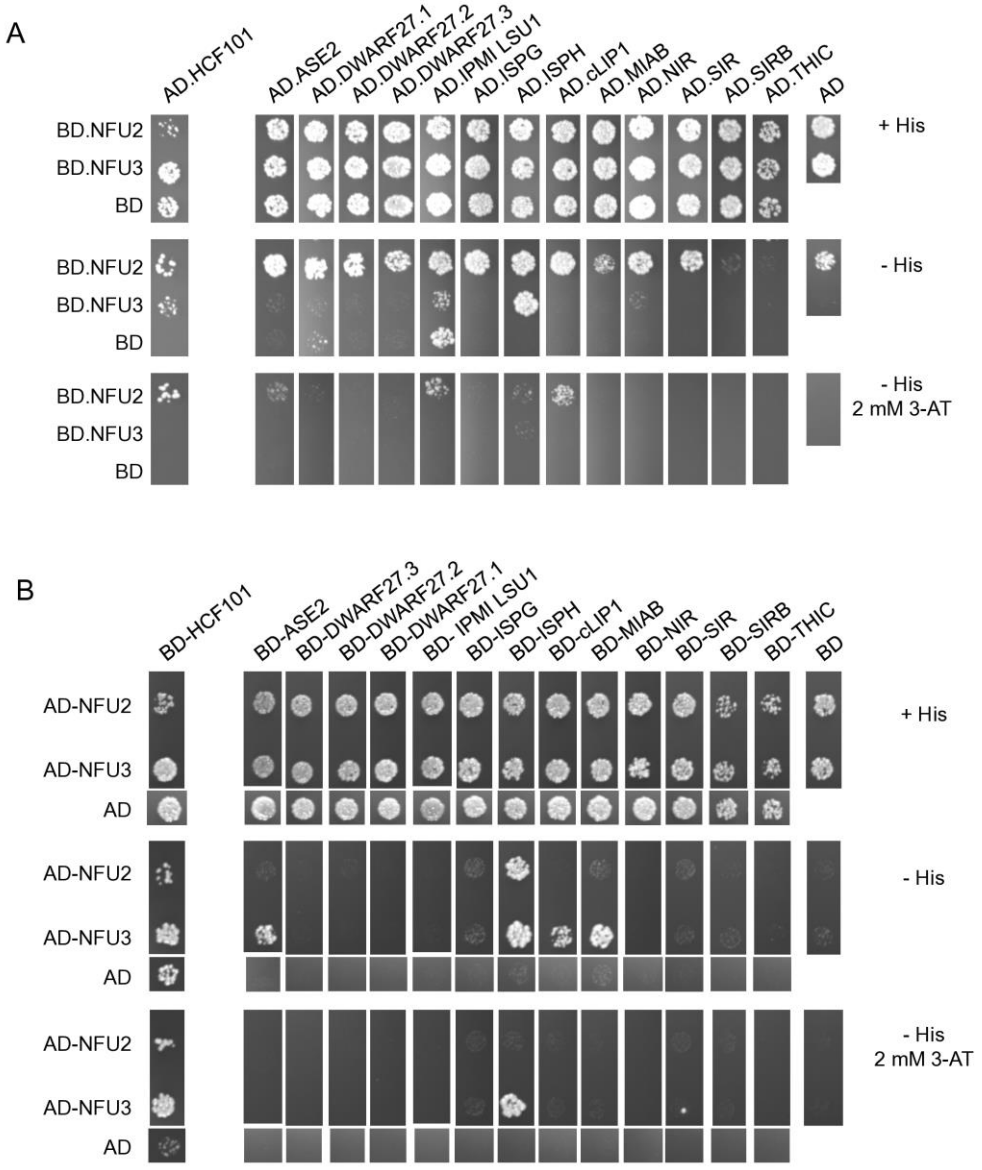

Figure 5. Yeast two-hybrid binary interaction screen between plastidial NFUs and selected [4Fe-4S]-containing proteins. Control plates contained histidine (+His) and test plates were without histidine (–His) in the absence or presence (2 mM) of 3-aminotriazol (+3AT). The images shown are representative of three independent transformation experiments. **(A)** Constructs expressing NFUs (NFU2 and NFU3) fused to the Gal4 DNA-binding domain (BD, NFUs used as baits) and **(B)** fused to the Gal4 activator domain (AD, NFUs used as preys). This figure is available in colour at JXB online.

Figure 6

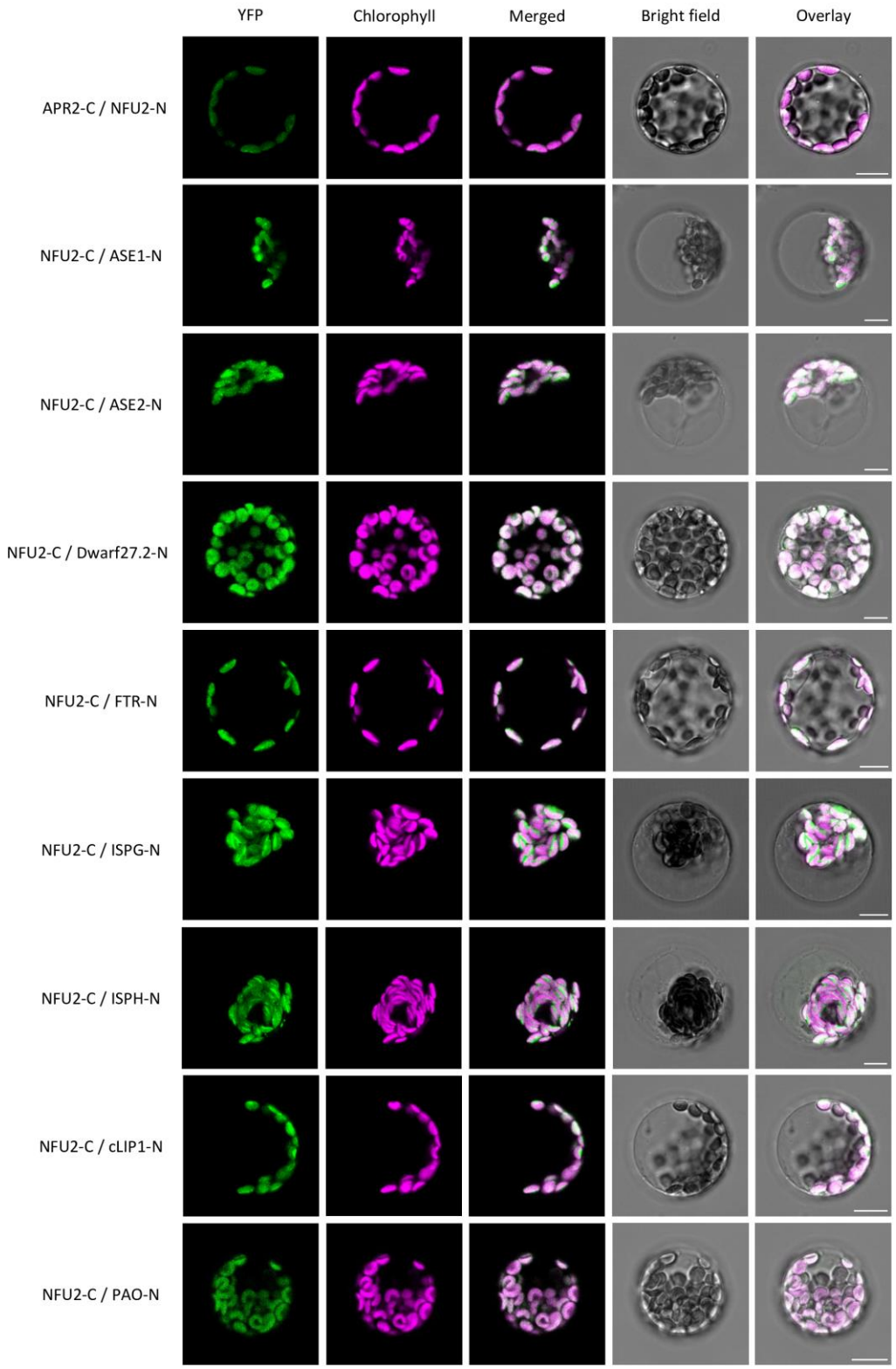

Figure 7